Geometrical factors determining dendritic domain intersection between neurons: a modeling study

Rafael Ignacio Gatica[1], Trinidad Montero[1], Navid Farassat[2] and Pablo Henny[1]

[1]Laboratorio de Neuroanatomía, Departamento de Anatomía, and Centro Interdisciplinario de Neurociencia, NeuroUC, Escuela de Medicina, Pontificia Universidad Católica de Chile, Santiago, Chile

[2]Institute for Neurophysiology, Goethe University, Frankfurt, Germany

*Corresponding author:

E-mail: pablohenny@uc.cl

ABSTRACT

Overlap between dendritic trees of neighboring neurons is a defining feature of central nervous systems. Dendritic domains sharing a given locus are arguably more likely to share afferent inputs, and proximity is a requirement for dendro-dendritic communication. Dendritic overlap also differentiates neuronal circuits characterized by redundancy and integration from those characterized by a more specific and selective connectivity. We examined the geometrical factors that affect intersection between pairs of neurons by, specifically, modelling the influence of cell-to-cell distance, and dendritic domain size and shape. We developed MATLAB scripts to determine intersected volume between pairs of three-dimensionally reconstructed neurons using their convex hull (CH) polyhedrons as proxies for dendritic domain. The influence of neuron-to-neuron distance on intersection was not straightforward and reflected the diverse and anisotropic geometry of neurons, and the ostensible displacement of cell bodies from the CH centroid. The influence of size on pair intersection was tested by giving each neuronal CH pair the same (average) volume without modifying their shape. Conversely, the influence of neuronal shape on pair intersection was proved by giving each neuronal pair an average shape without modifying volumes. While both normalization increased intersection, shape averaging was remarkably more effective than size averaging in increasing pair intersection. We conclude that intersection does not only depend on neuron-to-neuron proximity, but critically on neuron-to-neuron differences in size and shape. The results predict that circuits characterized by selective connectivity exhibit greater heterogeneity in size, but especially shape, of their constituent neuronal elements.

Author summary

Neurons communicate with each other using specialized domains called axons and dendrites. Throughout the brain, dendrites from adjacent neurons overlap. This dendritic overlap helps neurons to share common input information coming from axons and also permits communication between dendrites themselves. One way to study dendritic overlap is using the geometrical representation of the dendrites 'field of view', using simplified three-dimensional geometrical shapes (polyhedrons) called convex hulls. In this computational study, we used these convex hulls to analyze the geometrical factors underlying intersection between neurons. For that, we developed methods to obtain the intersected volume of pairs of convex hulls from neurons, to then independently modify the location, size and shape of convex hulls. We observed high variability in intersected volume, even when the neurons were at a similar distance between each other. Relevantly, we also found that variability in volume, but especially variability in convex hull shape is the main factor that determines the degree of intersection between pairs of neurons. These data suggest that differences in dendritic size, but especially differences in shape between neurons have a strong effect on overlap between neurons, and therefore on the potential for neurons to share input information and communicate with each other.

INTRODUCTION

Overlap between the dendritic trees of adjacent neurons is a characteristic found in virtually every region of the central nervous system across vertebrates [1–3]. Neurons whose respective dendrites share a given locus are likely to share common afferent inputs (Peters and Feldman, 1976, as discussed on [5]) and proximity between dendrites is an indispensable condition for synaptic [6,7] or paracrine-volume [8] dendro-dendritic communication. It follows that understanding the factors that influence intersection between adjacent are important to understand how information relay is organized from synaptic afferents to postsynaptic neurons within the brain and also how neurons within a given brain region communicate with each other. Indeed, intersection between adjacent dendritic or axonal fields has been mostly studied in primary neurons of the invertebrate somatosensory system, as well as in various retinal cell types. These studies have provided critical insights on receptive fields development, receptive field functional organization, and cell to cell communication [9–13].

A distinctive feature of the receptive domain of these sensory neurons is its two-dimensional organization, or at least its most relevant functional features. In this work, we wondered about the geometrical factors that affect volume intersection in central nervous system neurons, which in contrast to the above mentioned sensory neurons, have their receptive fields arranged three-dimensionally. Most central exhibit variable and complex geometries and sizes, and the disposition of the dendritic domain in relation to cell body position vary considerably even among neurons of the same type [14–16]. These traits imply that the geometrical determinants of intersection are more complex, and their analysis cannot rely on assumptions of shape circularity

or sphericity. Considering these factors, we sought to answer these simple questions: 1) How does the shape or size of dendritic domains affect intersection? 2) How does neuron to neuron proximity affect intersection? 3) How does the location of cell bodies within the dendritic domain affect intersection?

To address these questions, we used the 3D convex hulls of previously reconstructed neurons from the ventral tegmental area and substantia nigra [14]. Convex hulls are created joining the distal points of the dendritic tree to generate a polyhedron that encloses the minimal volume in which the dendritic domain of the neuron locates and therefore are used as a proxy of dendritic domain size and shape [14,16–21].

Hence, for this work we set the following aims: 1) to confirm the proof of principle that convex hull polyhedrons (CHP) are adequate proxies for dendritic space distribution by comparing CHP volume spatial distribution to dendritic length spatial distribution, 2) to adapt MATLAB scripts algorithms to estimate the intersecting volume between three dimensional CH, 3) to model the influence of cell body to cell body mediolateral (ML), dorsoventral (DV) and anteroposterior (AP) distances on intersected volume, 4) to model the influence of CH size and shape on intersection by comparing CH pair intersection using original with normalized CH volumes and shapes and, finally 5) to test whether these methodologies allow us to compare dendritic domain intersection dynamics between related but segregated populations such as those of the VTA and SNc.

RESULTS

CHP volume and intersection between CHPs pairs problem: method and validation

In this work, we developed methods to determine the intersected volume between the dendritic domain of pairs of adjacent neurons and further studied how the distance between neuronal pairs, as well as the size and shape of each respective dendritic domain affects how much their domains intersect.

A depiction of volume intersection between the dendritic domain of two neurons is shown in Fig 1A. The two reconstructed neurons were placed on their approximate position within the brain tegmentum [14]. When considering the CHP derived from the disposition of dendrites in space (Fig 1B) an intersected volume is defined (Fig 1C, more details in methods).

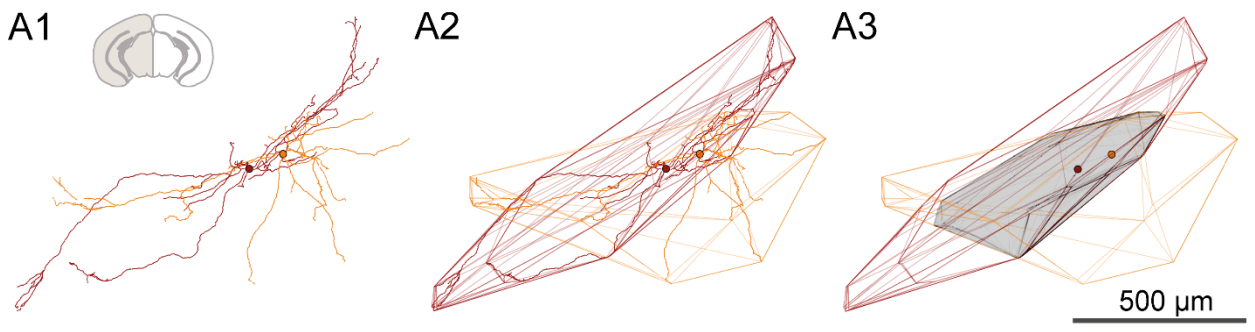

Fig 1. **Dendritic domain intersection.** A) A pair of reconstructed ventral tegmental area dopaminergic neurons (A1) and their corresponding CHPs (A2). Gray volume represents the intersected volume (A3). Cell bodies are represented with discs.

We started by validating the use of CHP as a proxy of the distribution of dendrites in space (Fig 2). For this, we used a sample of 15 tegmental neurons [14]. Specifically, we checked that the extent of a dendritic tree (measured in length) in the space surrounding the cell body (Fig 2A1) was proportional to the convex hull extension (measured in volume) in that particular space (Fig 2A2). For that we performed a wedge analysis (see Methods), dividing the dendritic field of each neuron into 4 anterior and 4 posterior quadrants, as centered on the cell body, and determined the proportion of dendritic length in each of these quadrants. We compared that to the proportion of CHP volume in each respective quadrant (Fig 2B) and found that there were no significant differences between these parameters (Two-way ANOVA Interaction: Anterior quadrants, $F_{(3,42)}$=0.4797 p=0.6981; Posterior quadrants, $F_{(3,42)}$=0.6734 p=0.5732), thus validating the use of CHP as an adequate proxy for the distribution of dendrites in space.

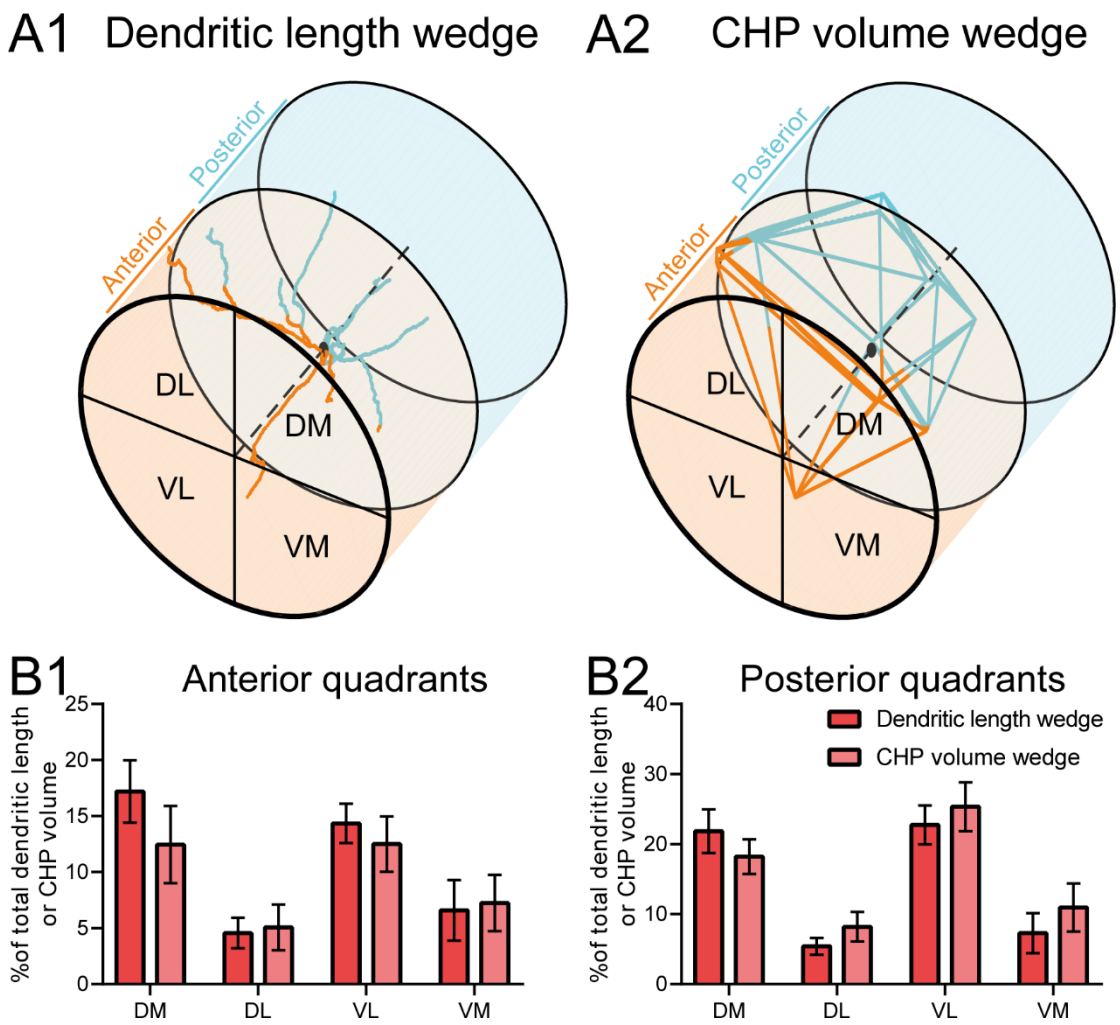

Fig 2. 3D wedge analysis for dendritic length and CHP volume distribution of ventral tegmental area (VTA) neurons. A) Schematic illustrating the 3D wedge analysis, with the cell body placed in the center of a cylinder (blue circle), which is divided into 4 angular wedges (dorsomedial, DM; dorsolateral, DL; ventrolateral, VL and ventromedial, VM) and 2 planes (posterior and anterior planes). The planes run perpendicular to the direction of the cylinder, creating 8 “quadrants”. Then, dendritic length is measured in each quadrant and normalized using the total dendritic length of the neuron (A1). For the CHP wedge analysis, the volume of the CHP in each quadrant is measured and normalized by the total CHP volume (A2). Dendrites or CHP edges inside the anterior or posterior plane were colored orange or cyan, respectively. B) Distribution of dendritic

133 trees and CHPs volume for tegmental dopaminergic neurons (n = 15 neurons). When a repeated
134 measures two-way ANOVA was performed within planes and within dendritic length and CHP
135 volume wedge, no significant differences were found: Interaction: $F_{(3,42)}$= 0.4797, p=0.6981 (B1);
136 $F_{(3,42)}$= 0.6734, p=0.5732 (B2). Bars represent mean ± SEM.
137

138 Influence of position, volume and shape on intersected domain: single
139 pair example

140 We developed scripts to determine the intersected volume between pairs of neuron's CHPs (S1
141 Fig, see Methods) and then studied the influence of each neuron position and geometry (size and
142 shape) on intersection. Because the intersected volume depends strongly on the volume of the
143 individual neurons involved (for instance, at an equivalent distance, the intersected volume of
144 two large but minimally intersected neurons could be the same as the intersected volume of two
145 small but largely intersected neurons), it was necessary to find a ratio (IR) that better represented
146 intersection. We defined this ratio to be the intersected volume divided by the non-intersected
147 volume. We normalized by the non-intersected volume (and not by the total added volume of
148 both individual neurons), so that the IR approached 100 (and not 50), for maximally overlapping
149 CHP.
150

151 We measured the IR for all possible pairs of 15 midbrain tegmental neurons as positioned in their
152 real observed location of their cell bodies within the brain (Montero et al., 2021, see Methods
153 section). The IR of all possible pairs (105, without repeating pairs) was calculated, and they were

154 plotted as a function of Euclidian distances between the pair of cell bodies (Fig 3A,B). As
155 expected, the further away from the cell bodies, the lower the IR. However, high variability in IR
156 can be observed at equivalent distances between the pairs' cell bodies. As an illustrative example,
157 Fig 3A shows two neuronal pairs (highlighted in red in 3B) with their respective cell bodies
158 separated by a similar distance (around 200 µm). Yet the IR of pair A (24.9%) is ostensibly higher
159 than CHP pair B (1.5%). High variability was also observed when we plotted intersected volume
160 (mm^3) instead of IR (S2B Fig). These results indicate that IR between neuronal pairs depends on
161 the distance between their cell bodies, but also on other geometrical characteristics.
162

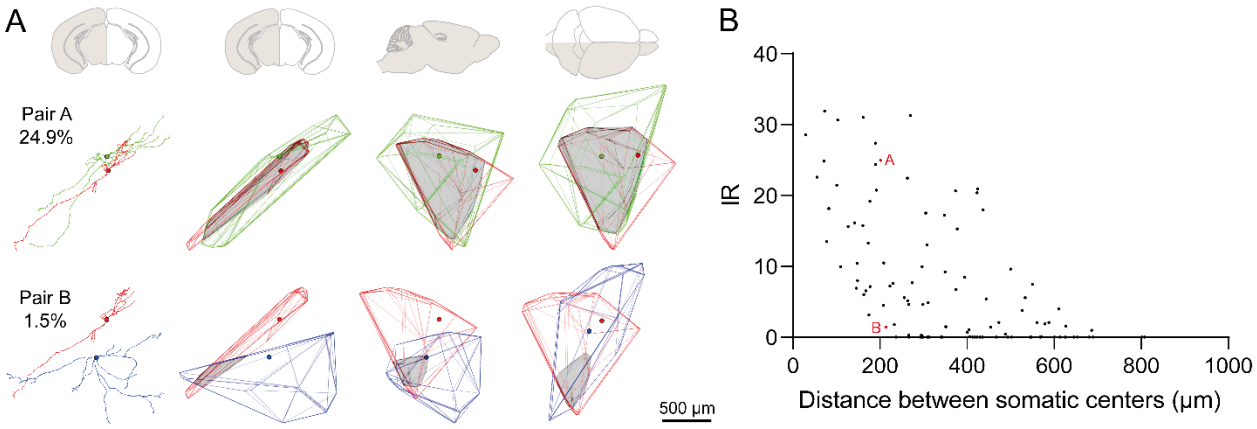

163

164 **Fig 3. IR variability from a sample of tegmental neurons as located in their approximate location**
165 **within the brain ventral tegmental area.** A) Representative examples of neurons and their CHPs,
166 as observed from the frontal, lateral and dorsal view. At a similar distance between cell bodies,
167 CHP pair A showed a higher IR than CHP pair B, respectively. These examples are highlighted in
168 figure B (red points and letters). Gray volume represents intersected volume. Cell bodies are
169 represented with discs. B) IR values between pairs of CHPs, as measured in their corresponding
170 position. Each point represents the IR value of a pair of CHPs (105 pairs tested).

To understand how the differences in geometry between neuronal pairs influence intersection, we systematically modeled the influence of neuron-to-neuron distance, and neuron-to-neuron differences in volume and shape, using the cell body as the center of each neuron. Specifically, we tested how neuron-to-neuron distance influenced IR values when: 1) the original volume and shape of each neuron were used, 2) the shape of each neuron was maintained but an average volume was used instead, 3) the volume of each neuron was maintained but an *average* shape was used, and 4) the average volume and average shape were used for both neurons. We first modeled a single pair of neurons to illustrate the procedure, but also to study the effect of distance, volume and shape on intersection in a simpler situation (Figs 4-8). Then, the analysis was extended to a larger sample of neurons (Fig 9-11).

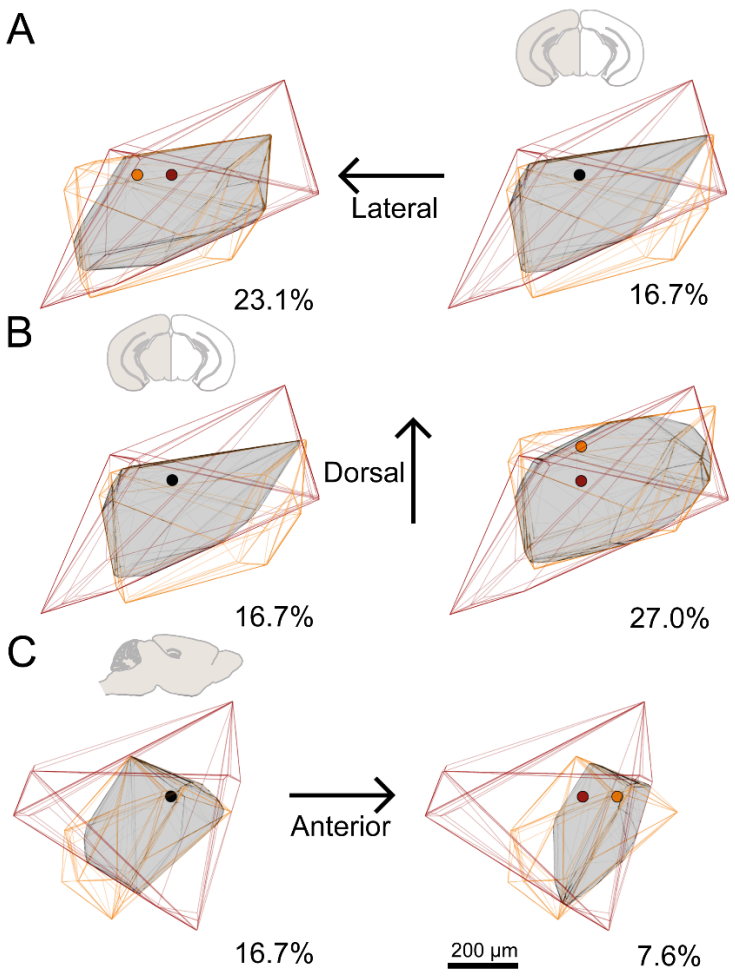

Fig 4. Original volume - original shape analysis. A-C) A representative example of IR measurement when the distance between pairs of neurons CHPs was 0 µm or 100 µm across the ML (A, frontal view), DV (B, frontal view), and AP (C, lateral view) axis. Cell bodies are represented with discs.

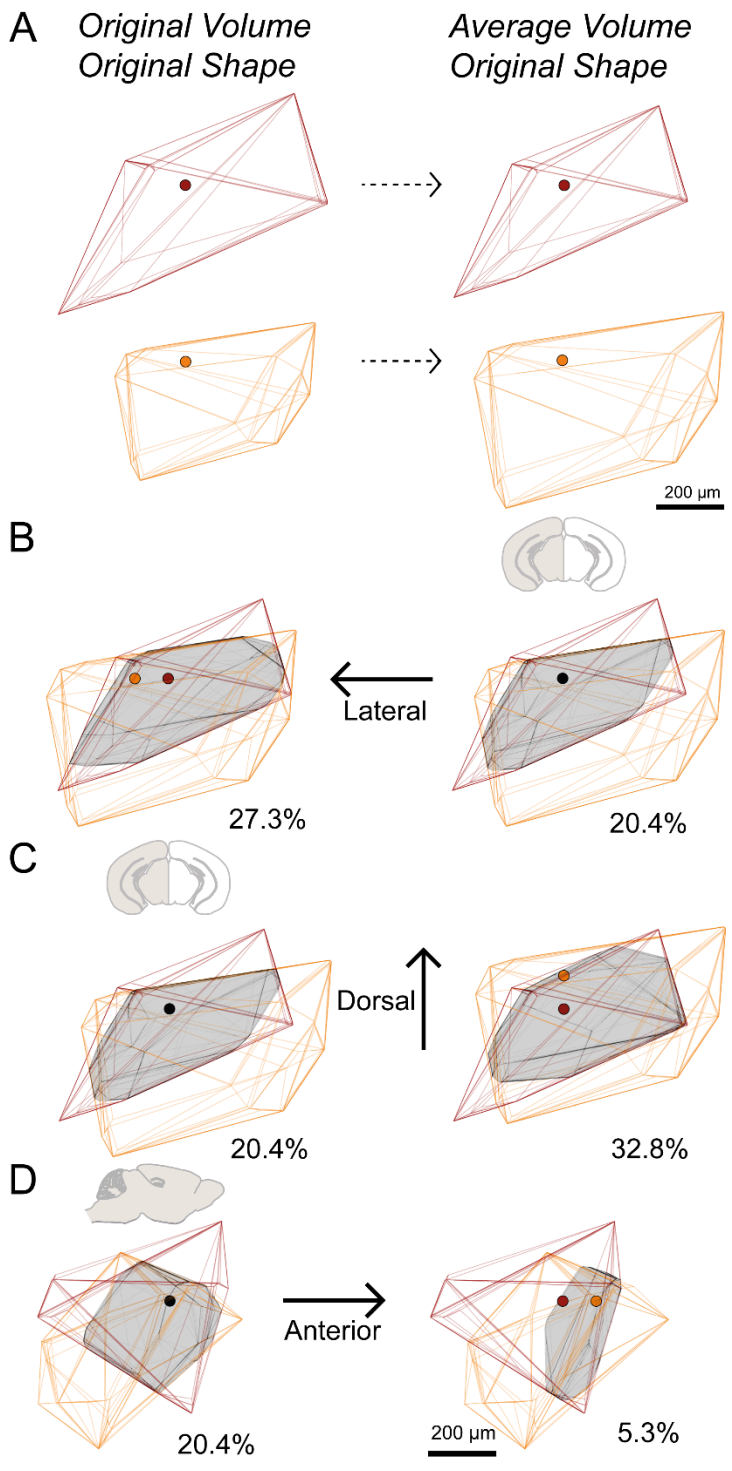

Fig 5. Average volume - original shape transformation and analysis. A) Same pair of CHP as in Figure 4. Volume was modified for both CHP to 0.045 mm^3 (average value for the pair of neurons). B-D) IR was measured when the distance between pairs of CHPs was 0 µm or 100 µm across the

191 ML (B, frontal view), DV (C, frontal view), and AP (D, lateral view) axis. Cell bodies are represented

192 with discs.

193

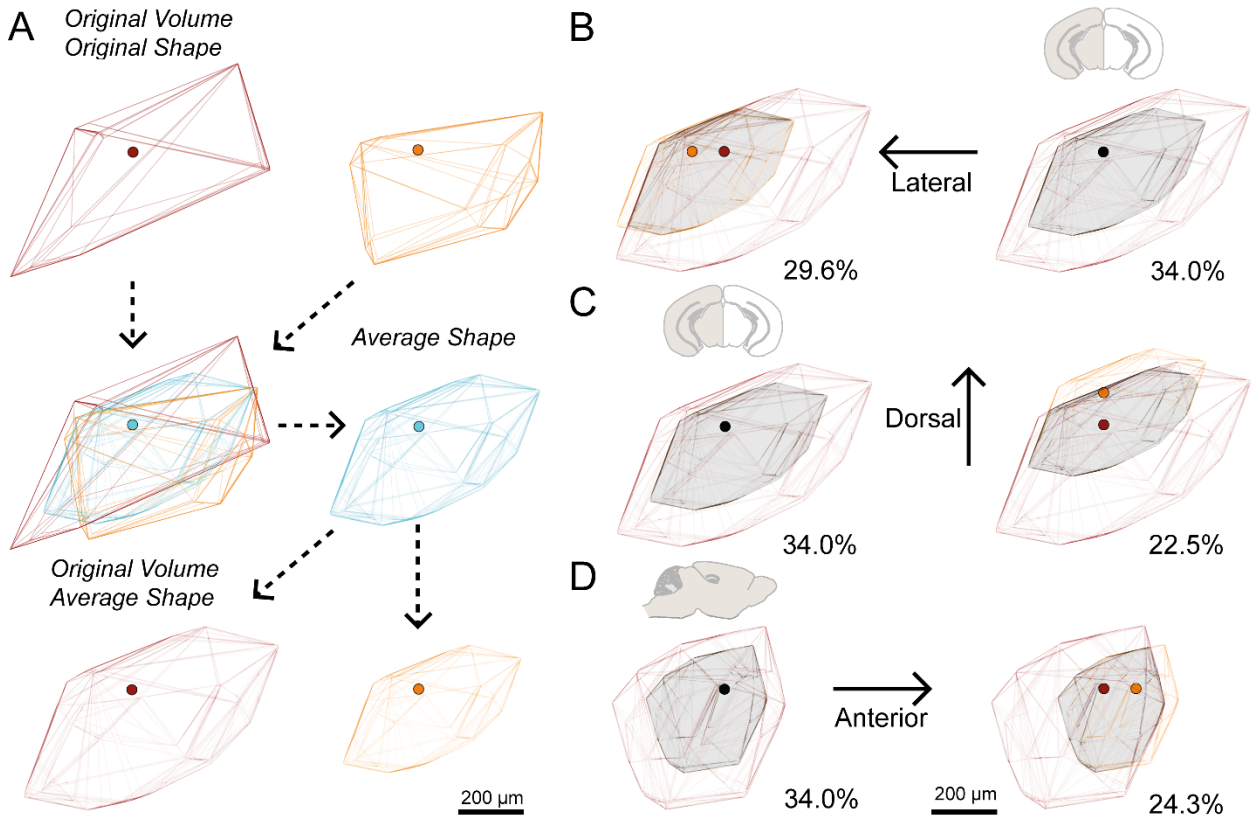

194

195 **Fig 6. Original volume - average shape transformation and analysis.** A) Same pair of CHPs as in

196 Figure 4 (top row), were aligned around their cell bodies and the average CHP shape was obtained

197 (cyan, middle row). Using this average CHP, new CHPs were created using the volumes of the

198 original CHPs (bottom row). B-D) IR was measured when the distance between pairs of CHPs was

199 0 µm or 100 µm across the ML (B, frontal view), DV (C, frontal view), and AP (D, lateral view) axis.

200 Cell bodies are represented with discs.

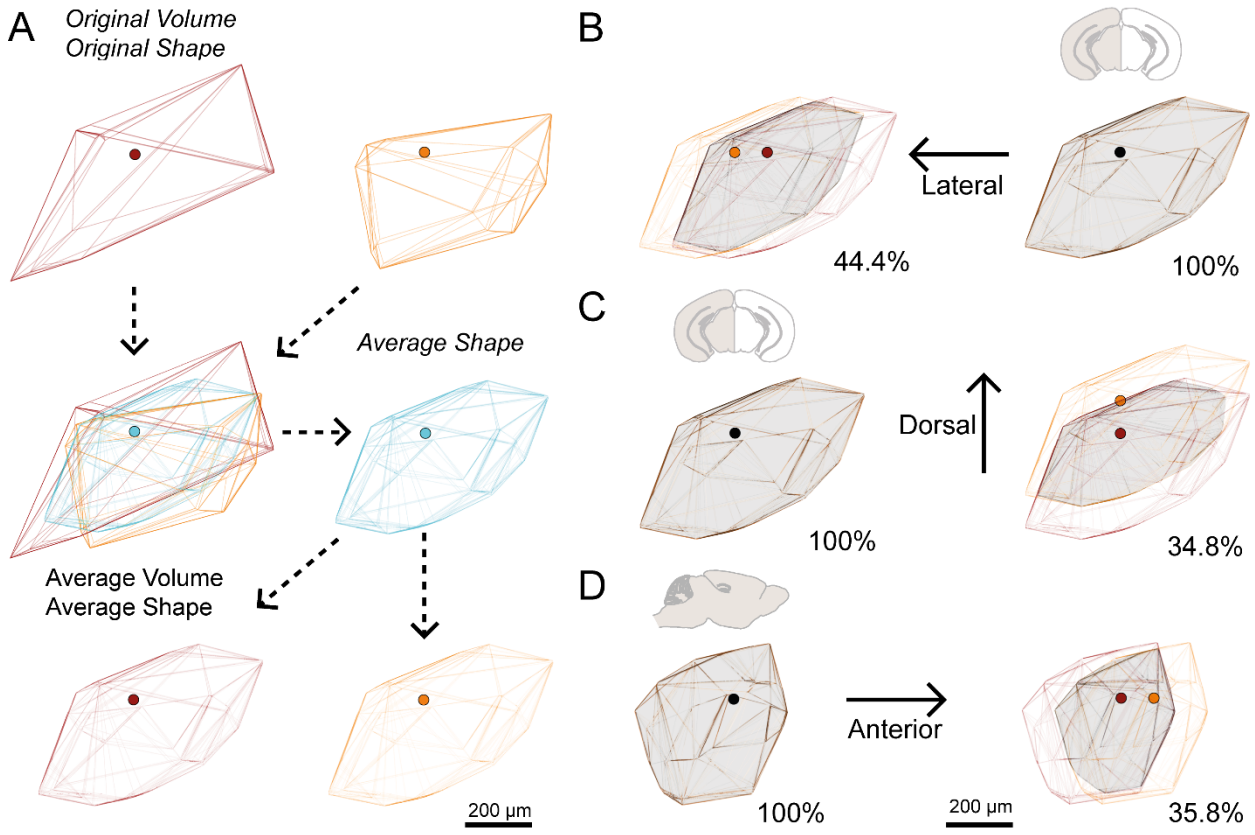

Fig 7. Average volume - average shape transformation and analysis. A) Same pair of CHPs as in Figure 4 (top row) were aligned around their cell bodies and the average CHP shape was obtained (middle row, cyan). Using this average CHP, new CHPs were created using a volume of 0.045 mm^3 (average value for the pair of neurons, bottom row). B-D) IR was measured when the distance between pairs of CHPs was 0 µm or 100 µm across the ML (B, frontal view), DV (C, frontal view), and AP (D, lateral view) axis. Cell bodies are represented with discs.

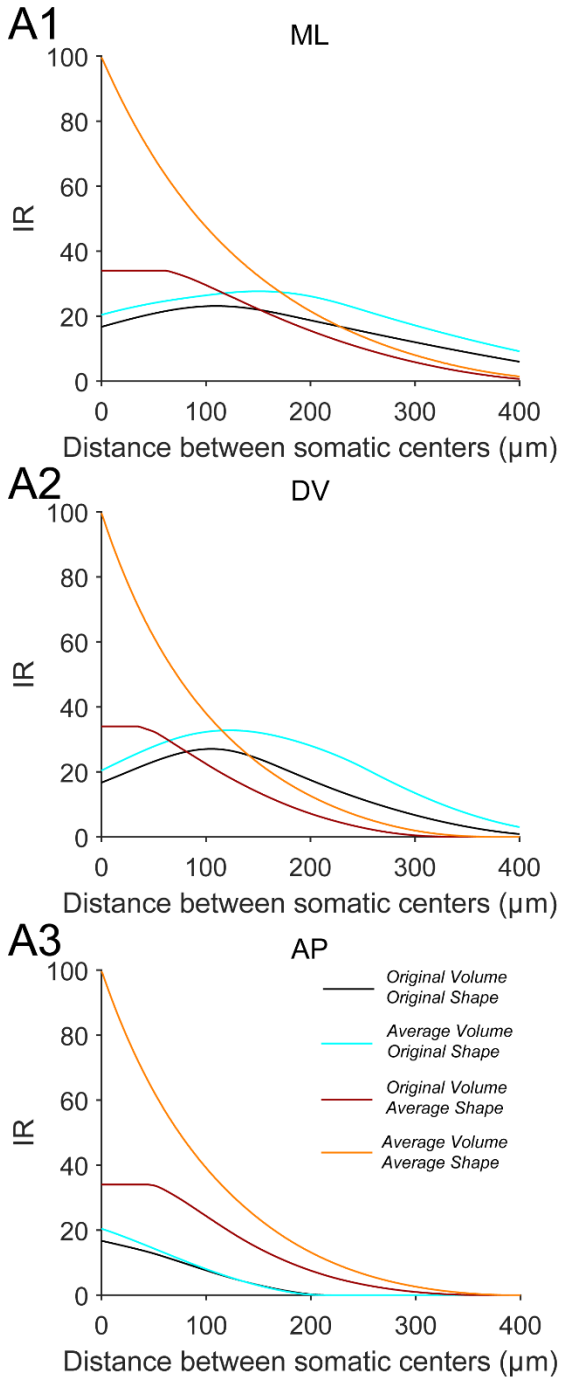

Fig 8. Comparison between CHP modeling conditions for a single pair (same as in Figures 4-7). Effect of distance between cell bodies on IR of the pair of CHPs used in Figures 4-7. IR was measured between 0 to 400 µm (1 µm steps) within the ML (A1), DV (A2), and AP (A3) axis.

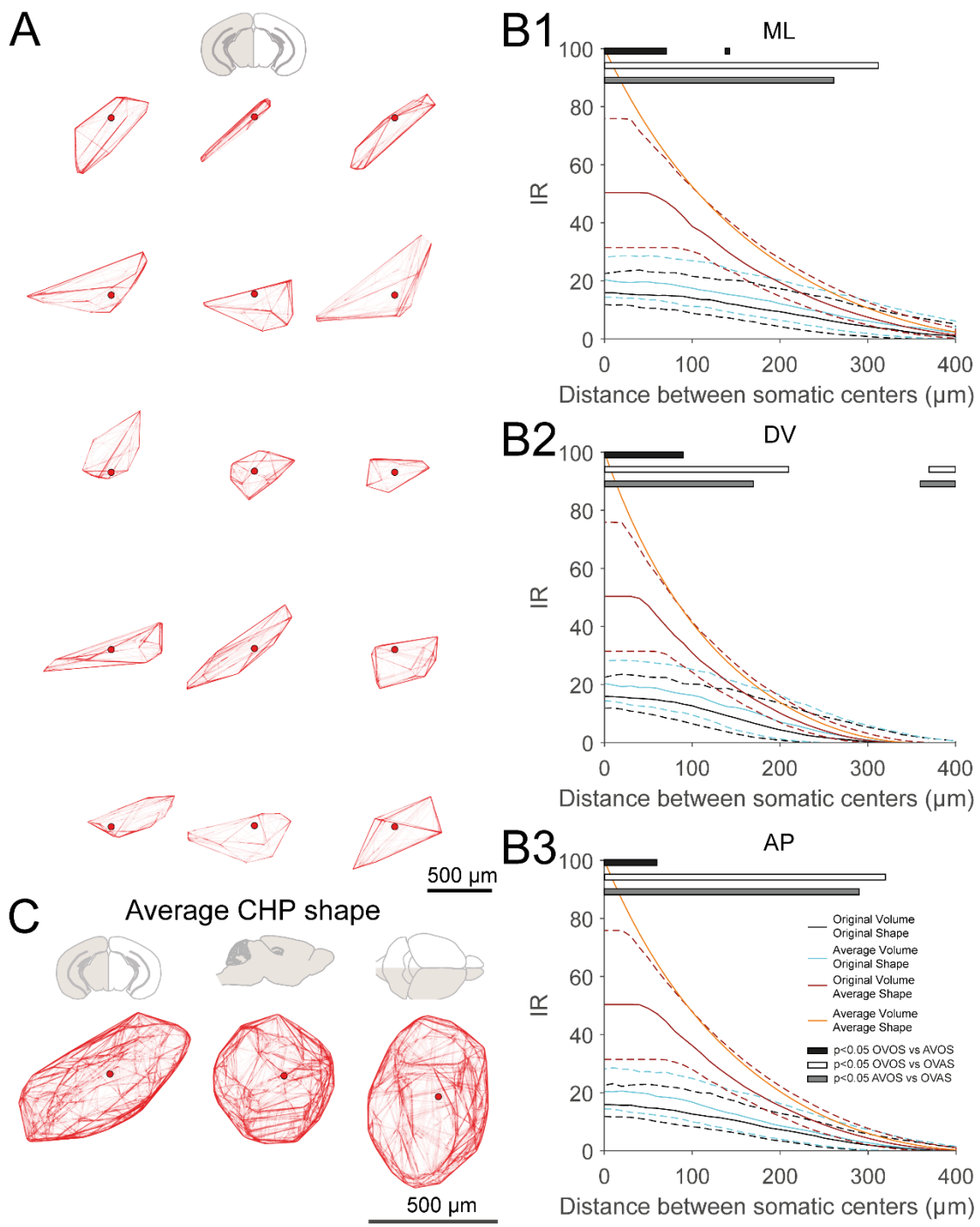

Fig 9. CHP modeling for tegmental neurons: within regions comparison. A) All CHPs of tegmental neurons used in this study (n = 15, frontal view only). Cell bodies are represented with discs. B) Analysis for original volume - original shape (OVOS), average volume - original shape (AVOS), original volume - average shape (OVAS) and average volume - average shape (AVAS) conditions

218 were performed for all the possible pairs from a sample of tegmental neurons (210 pairs per
219 distance, except for AVAS, were n=1), and compared within areas. IR was measured between 0
220 to 400 µm (10 µm steps) within the ML (B1), DV (B2), and AP (B3) axis in each area. Average
221 volume = 0.047 mm^3 (CHP volume average for nigral neurons). Statistical analyses were
222 performed using a Friedman test, followed by a Dunn-Sidak post-test. A horizontal line depicts
223 the significant differences ($p<0.05$) between OVOS vs AVOS (top black significance lines), OVOS
224 vs OVAS (top white significance lines) and AVOS vs OVAS (top gray significance lines). Solid line
225 represents the median. Upper and lower dashed lines represent the 75th and 25th percentile,
226 respectively (except for AVAS, were n=1). C) Average CHP shape of tegmental neurons, as
227 observed from the frontal, lateral and dorsal view. Cell bodies are represented with discs.

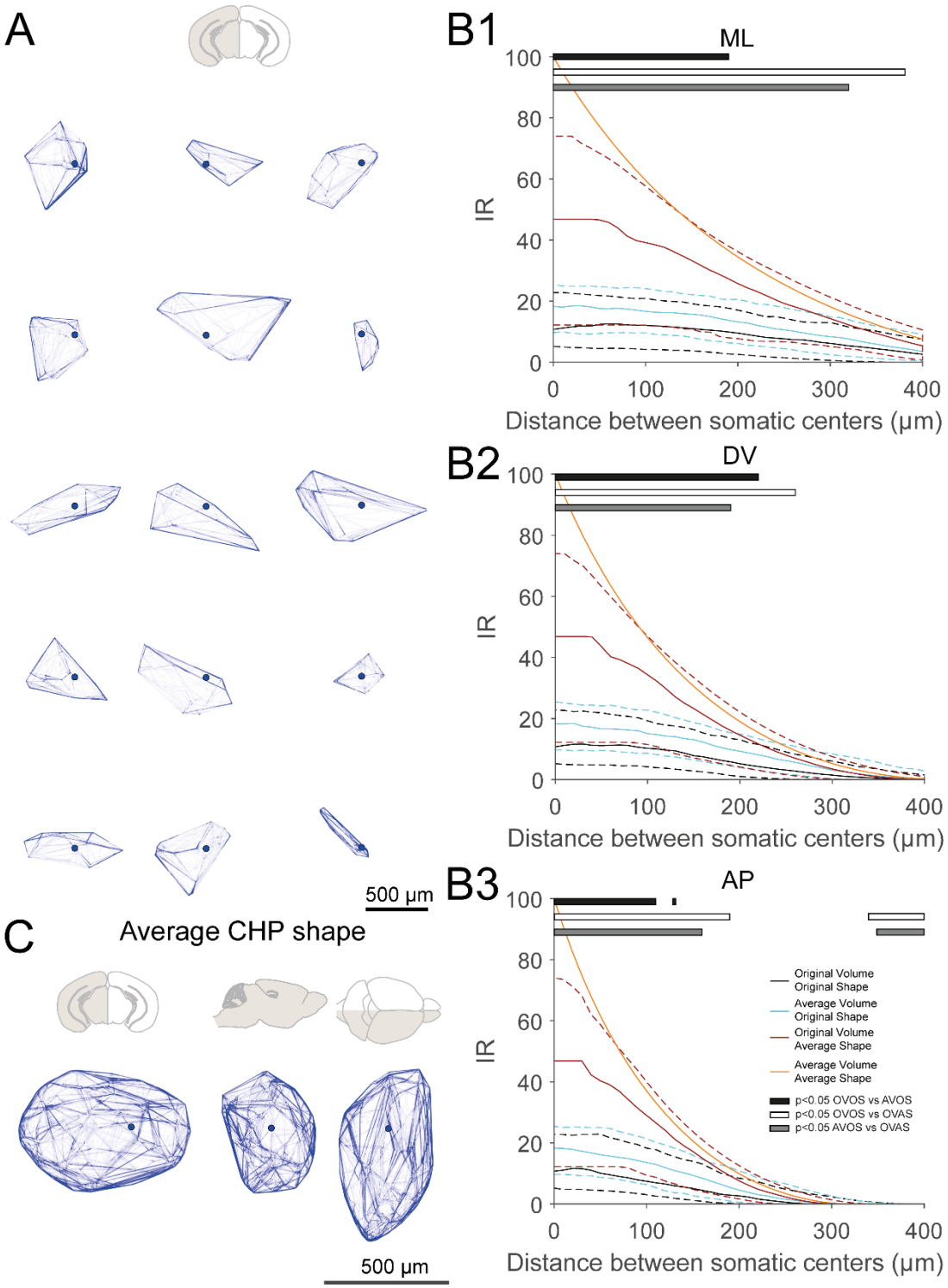

Fig 10. **CHP modeling for nigral neurons: within regions comparison.** A) All CHPs of nigral neurons used in this study (n = 15, frontal view only). Cell bodies are represented with discs. B) Analysis for original volume - original shape (OVOS), average volume - original shape (AVOS),

232 original volume - average shape (OVAS) and average volume - average shape (AVAS) conditions
233 were performed for all the possible pairs from a sample of nigral neurons (210 pairs per distance,
234 except for AVAS, were n=1), and compared within areas. IR was measured between 0 to 400 µm
235 (10 µm steps) within the ML (B1), DV (B2), and AP (B3) axis in each area. Average volume = 0.042
236 mm^3 (CHP volume average for nigral neurons). Statistical analyses were performed using a
237 Friedman test, followed by a Dunn-Sidak post-test. A horizontal line depicts the significant
238 differences ($p<0.05$) between OVOS vs AVOS (top black significance lines), OVOS vs OVAS (top
239 white significance lines) and AVOS vs OVAS (top gray significance lines). Solid line represents the
240 median. Upper and lower dashed lines represent the 75th and 25th percentile, respectively (except
241 for AVAS, were n=1). C) Average CHP shape of nigral neurons, as observed from the frontal, lateral
242 and dorsal view. Cell bodies are represented with discs.

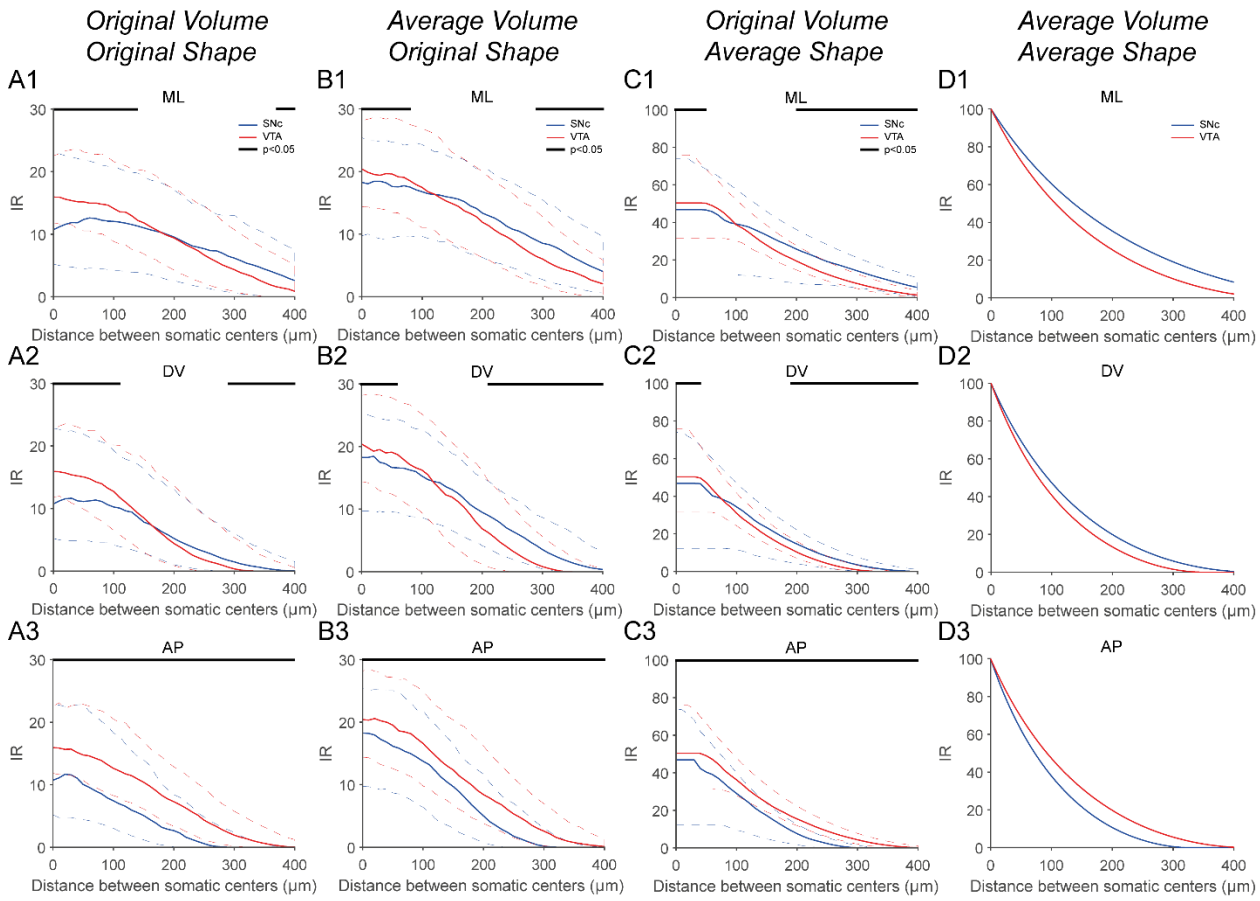

Fig 11. Population analysis of CHP modeling: between regions comparison. Original volume - original shape (A), average volume - original shape (B), original volume - average shape (C) and average volume - average shape (D) analysis were performed for all the possible pairs from a sample of SNc and VTA dopaminergic neurons (210 pairs per distance, except for average volume, average shape were n=1), and compared between areas. IR was measured between 0 to 400 µm (10 µm increases) within the ML (A1, D1), DV (A2, D2), and AP (A3, D3) axis in each area. Average volume = 0.045 mm^3 (CHP volume average of nigral + tegmental neurons). Statistical analyses were performed using a Wilcoxon rank sum test. A horizontal line depicts the significant differences ($p<0.05$) between SNc and VTA. Solid line represents the median. Upper and lower dashed lines represent the 75th and 25th percentile, respectively (except for AVAS, were n=1).

254

255 We started studying intersection (IR) as a function of distance using the original volumes and
256 shapes of a pair of neurons (original volume – original shape condition). For that, we placed the
257 cell bodies of the pair of neurons on the origin of a 3D space (coordinate 0, 0, 0), and then
258 displaced the cell body of one of them 100 µm laterally (Fig 4A), dorsally (Fig 4B) or anteriorly
259 (Fig 4C) on the ML, DV and AP axes respectively. As it can be observed, IR depended on the axis
260 on which the neurons were displaced. For instance, the pair in Fig 4 shows over 16% of
261 intersection at 0 um distance, but when displaced 100 um laterally, dorsally or anteriorly, IR
262 values change to 23%, 27% and 8%, respectively. It is noticeably that a 100 um separation of cell
263 bodies in lateral and dorsal directions actually results in higher IR values than when centered
264 around their cell bodies, illustrating for this pair of neurons and distance tested, the complex
265 relation between proximity and intersection between neuronal pairs.

266

267 We then explored how differences in volume between pairs of neuronal CHP affects IR. We
268 reasoned that the effect of volume on IR could be studied by controlling for volume, i.e., by
269 comparing the IR values when original and average volumes were used. We took the same pair
270 of CHP as in Fig 4 and changed the volume of each neuronal CHP to the average volume between
271 the two (approximately 0.045 mm^3, Fig 5A). As in Fig 4, we aligned the cell bodies of the same
272 pair (coordinate 0, 0, 0) and then displaced the cell body of one of them 100 µm laterally (Fig 5B),
273 dorsally (Fig 5C) and anteriorly (Fig 5D) on the ML, DV and AP axes respectively. We found that
274 using an average volume resulted in increased IR values lateral or dorsal displacements (as

275 compared to the original volume - original shape condition, Fig 4) and a slight decrease in IR when
276 displaced anteriorly.
277
278 To address the effect of differences in CHP shape on IR we reasoned that, similarly, this could be
279 assessed using an *average* shape for both neuronal CHP. We set to find a CHP that, as explained
280 in detail in the Methods section and S3 Fig, we defined as the CHP of the polyhedron formed by
281 the points located at mid-distance between the surfaces of two or more CHP, with their cell
282 bodies aligned. We used the same neurons from Fig 4 and generated the average CHP for this
283 particular pair. Then, we restored the original volume for each neuron of the pair (Fig 6A). As in
284 previous figures, we displaced the neuron 100 um laterally, dorsally or anteriorly (Fig 6B-D).
285 Critically, we found that, in contrast to the original volume - original shape condition (Fig 4) or to
286 the average volume – original shape condition (Fig 5), using an average shape (while keeping the
287 original volume) in this pair, a 100 um displacement resulted in IR values that decreased (Fig 6)
288 in all axes.
289
290 Finally, we tested IR using both average volume and average shape (Fig 7, average volume -
291 average shape). In this case, given that the pair of CHP would be identical, IR was maximal at 0
292 µm and decreases at 100 um in each axis. Again, in contrast the original volume – original shape
293 or average volume – original shape conditions, and similarly to the original volume – average
294 shape condition, all IR values decreased when displaced 100 um, in all axes (Fig 7).
295

296 We decided to examine intersection dynamics more systematically by testing the effect of
297 distance on IR at 0 – 400 um in 1 um steps. In this way, we were able to compare the effect of
298 volume and shape in terms of distance-versus-IR curves.
299
300 As seen in Fig 8 (black curves), the original volume - original shape condition, confirmed that the
301 relation between IR and CHP position depended on the axis on which the CHP were displaced.
302 For instance, for this tested pair of CHPs the IR was not decremental for all distances ranges. On
303 the one hand IR values show a substantial increment for both lateral (ML axis) and dorsal (DV
304 axis) displacements (hill-shaped or U inverted shape curve), whereas anterior displacement (AP
305 axis) resulted in a continuous decrement. When testing IR with the neuronal pair having a
306 common volume (average volume - original shape condition, cyan curves), we observed an
307 increase in IR values for each tested distance. On the other hand, the overall dependency of IR
308 to distance (the shape of the curves) was maintained. In contrast, the use of a common shape
309 (original volume - average shape condition, dark red curves) showed a much more pronounced
310 effect on distance versus IR curves. To start with, IR curves in ML and DV axes are no longer hill-
311 shaped and show much higher values at closer distances and in fact, all curves start with an initial
312 plateau, reflecting that one CHP is inside the other CHP. In other words, normalizing shape not
313 only increases intersection but, overall, it changes the way intersection depends on distance.
314 Finally, the use of a common shape and common volume (average volume – average shape
315 condition, orange curves), which is equivalent to compare two identical CHPs, showed maximal
316 at 0 µm and a decremental relation for all distances and axes tested.
317

318 In summary, these results illustrate the complex relationship between distance and intersection,
319 reflecting the anisotropic shape as well as the displaced location of the cell body in relation to
320 the CHPs centroid. Results also suggest that initial shape differences have a much larger effect
321 than volume differences volume on IR.
322

323 Influence of position, volume and shape on intersected domain: 324 population analysis

325 By using a pair of neurons as a representative example, we just described how position, volume,
326 and shape modifies intersection. To have a more ample view of intersection dynamics within a
327 brain population, we extended our analysis to 15 neurons of the same tegmental region (the VTA,
328 Fig 9A) and analyzed their geometry and the rules underlying intersection.
329
330 As it can be seen in Fig 9A, we obtained the CHP of those 15 neurons and found that CHPs were
331 not only diverse in size (Montero et al., 2021) and shape, but also on the location of the cell body
332 within CHP (circles). In the same way, as for the single pair of neurons shown in Fig 8, we studied
333 IR as a function of position for all possible pairs for those 15 neurons (210 pairs in total (15 *
334 (15-1) = 210) this time repeating pairs, because a neuron in a pair was first tested moving to one
335 orientation of the axis, and then the other).
336
337 We first tested the original volume - original shape volume condition (Fig 9B, black curve) and
338 observed, as expected, that distance decreases IR, yet exhibiting a slight plateau at relatively

339 close distances (0 – 100 um). Then we tested the average volume – original shape condition using
340 the average volume of all tegmental neurons sampled (0.047 mm^3, see Methods) and found that
341 IR increased as tested in the three axes (cyan curves).
342
343 In order to provide the average shape, we applied the transformation described for the single
344 pair of neurons of Figs 6 and 7, but for all tegmental neurons CHPs. The process resulted in an
345 average shape that is presented in Fig 9C. As it can be appreciated, the average shape exhibits
346 the essential geometrical features of this dopaminergic population, particularly the dendritic
347 domain size and the extension in the ML, DV and AP axes. In frontal view, we observe that the
348 CHP was oriented dorsomedially to ventrolaterally, with the cell body at mid position, in
349 agreement with the distribution of VTA neurons dendritic field, as described in (Montero et al.,
350 2021). We confirmed that distribution of volume around the cell body for this average CHP was
351 equivalent to that found for all CHPs in the wedge analysis from Fig 2 (Anterior: DM=11.06%,
352 DL=4.82%, VL=14.54%, VM=6.60%; Posterior: DM=17.76%, DL=7.78%, VL=26.75%, VM=9.80%).
353
354 Fig 9B (dark red curves) shows the effect that averaging shape (original volume – average shape)
355 has on distance versus IR curves, which show much higher values than both the original volume
356 – original shape and average volume – original shape conditions, in the three axes tested. The
357 average volume – average shape condition, as also observed in Fig 8 for the single CHP pair,
358 showed maximal values at every distance and axis tested.
359

360 We extended our analysis to a related population of neurons and examined whether intersection
361 dynamics were similar. For that, we took 15 nigral neurons (Montero et al., 2021) and obtained
362 their CHP (Fig 10A). We confirmed that CHP was a good proxy for dendritic distribution in nigral
363 neurons, repeating the wedge analysis of Fig 2 and found that volume distribution for individual
364 CHP did not differ from dendritic length distribution (S4A Fig, Two-way ANOVA interaction: SNc
365 Anterior quadrant, $F_{(3,42)}$=0.2566 p=0.8562; SNc Posterior quadrant, $F_{(3,42)}$=0.9138 p=0.4425). We
366 confirmed high variability in IR values as a function of Euclidian distances from the real observed
367 location of nigral neurons within the brain (Montero et al., 2021, see Methods section). As for
368 tegmental neurons (Fig 3A and B), the IR of all possible pairs of nigral neurons (15 * (15 – 1)) / 2)
369 = 105) was calculated, and they were plotted as a function of Euclidian distances between the
370 pair of cell bodies (S4B,C Fig), indicating, again, that geometrical factors have a great influence
371 on intersection. Finally, we also obtained the average CHP (Fig 10C) and found the typical
372 dorsolateral to ventromedial orientation of nigral neurons [14] and the cell body displaced
373 medially, while its location seems to be more central regarding AP position (seen in frontal and
374 lateral views), in agreement with the described distribution of nigral neurons dendritic field (S4A
375 Fig). Relevantly, average CHP volume wedge for nigral neurons, was similar to the values found
376 for dendritic length and CHP volume wedge from S4A Fig (Anterior: DM=5.86%, DL=12.92%,
377 VL=19.16%, VM=10.43%; Posterior: DM=5.47%, DL=20.04%, VL=19.93%, VM=5.20%).
378
379 Results showed that IR curves dynamics of IR curves in the 3 axes for nigral neurons were similar
380 to VTA tegmental neurons (Fig 10B). Interestingly, original volume – original shape (black curves)
381 exhibited a slight but consistent IR maximal near 100 um, similar to what was observed for the

382 single pair example of Fig 8. For average volume computations, the average CHP volume for our
383 sample of nigral neurons was 0.042 mm^3. Similar to VTA neurons, we also observed that
384 averaging shape (dark red curves) increased IR values when compared to the original volume –
385 original shape condition, but especially compared to the average volume – original shape
386 condition (cyan curves). Thus, these results confirm that CHP shape variability is the main factor
387 determining IR between neuronal pairs.
388

389 ## Intersection dynamics between tegmental and nigral populations

390 Finally, we compared tegmental and nigral populations in each of the four tested conditions (Fig
391 11). For original volume - original shape condition (Fig 11A), tegmental neurons showed higher
392 IR values than nigral neurons at shorter distances in the ML and DV axis and across all the tested
393 distances in the AP axis, while at larger distances between cell bodies, nigral neurons showed
394 higher IR values than tegmental neurons in ML and DV axis.
395

396 Regarding average volume - original shape, some differences were evidenced between the two
397 populations (Fig 11B). Here, we obtained the average CHP volume taking together both nigral
398 and tegmental neurons values, with the value being equal to 0.045 mm^3. Although for VTA
399 tegmental neurons IR values were higher than nigral neurons in ML and DV, they were observed
400 at fewer distances than in original volume - original shape condition. Moreover, nigral neurons
401 showed significant differences at more distances than VTA at larger distances compared to
402 original volume - original shape condition. Regarding the AP axis, VTA neurons continued to show
403 higher IR values than nigral neurons in all tested distances.

In the original volume - average shape condition, both populations showed higher IR values than in the average volume - original shape condition, yet curves for both areas were similar in the ML and DV axes (Fig 11C). Regarding the AP axis, VTA neurons still showed higher IR values than SNc in all tested distances.

Finally, in the average volume - average shape condition, considering that only one pair of CHPs is tested, differences between areas were assessed by testing whether in each axis the data fitted to the same curve or not (Fig 11D). In this case, an exponential decay model was applied. In each axis, higher R^2 values (>0.99) were found when the data of each area was fitted alone than when data of both tegmental and nigral populations were pooled together. This means that, for each axis, a significant difference between curves was found. Then, our results showed that in ML and DV axes, the nigral population curves were higher than tegmental neurons curves, whereas the tegmental neurons curve was higher than the nigral curve in the AP axis.

Overall, these results highlight that differences in CHP shape and position allow to determine differences in intersection between the dendritic fields of differentiated brain populations (tegmental VTA and nigral SNc) dopaminergic neurons.

423 # DISCUSSION

424 In this study we developed computational tools to estimate the volume generated by the
425 intersection of two adjacent neurons' dendritic domains. Using CHPs as a proxy for dendritic
426 domain size and shape, we modeled the effect of neuron-to-neuron proximity in a three-
427 dimensional space and the effect of dendritic domain volume and shape of individual neurons on
428 intersection. Our results show that the rules governing geometrical intersection between
429 neurons are complex, reflecting the anisotropic shape of neuron's dendritic domain as well as
430 the displaced location of the cell body inside it. Results also show that differences in dendritic
431 domain size, but especially differences in its shape increase exclusion (i.e. decrease intersection)
432 between adjacent neurons. In the following sections, we discuss the methodological challenges
433 involved in this study as well as the biological significance of these findings.

434

435 Computational tools to find an intersected region have been developed before for pairs of convex
436 polygons [22,23] and polyhedrons [22,24,25]. Yet to the best of our knowledge this is the first
437 attempt to use these tools to study overlap in 3D-structured neurons. In fact, with few exceptions
438 [26,27], studies on overlap between nervous structures have been carried out on peripheral
439 somatosensory or visual systems neurons, focusing on the (2D) surface covering properties of
440 receptive fields formed by dendrites or nerve terminals [11]. In addition, studies have usually
441 focused on the average overlap between neurons of a receptive field [9,10,12,13], but not on the
442 specific geometrical properties that finally determine receptive field overlap for a given
443 population. Thus a first step in this work was to develop tools to determine the intersected

volume between CHPs efficiently (S1 and S5 Figs), which in turn allowed us to model the effects of 3D geometry on intersection.

In order to study the influence of shape on intersection (see below), an additional challenge in this study was to find an average shape of two or more CHP which fulfilled the need of being theoretically sensible and practically useful. We defined the average CHP as the CHP of a polyhedron formed by the points located at mid-distance between the surfaces of two or more CHP with their cell bodies aligned. The solution evokes that of graphic morphing or metamorphosis used in computational graphics to provide smooth transition between two different shapes using intermediate steps [28–31]. In that sense, the average CHP could be seen as analogous to an intermediate step shape. The difference between the morphing approach and ours, however, is that in some morphing approaches specific (correspondent) points are defined as *a priori* landmarks and can work as a pivot (for instance the eyes when morphing from one face to another) [32], whereas in our solution the there are no landmarks to pivot on. Thus, our *intermediate* step shape can be seen as a true *average shape*.

The use of neurons' convex hull to represent dendritic distribution poses the question of the extent to which it represents a meaningful proxy for dendritic domain size, shape, or even function in 3D space. In fact, the vast majority of space within a neuronal CHP is not occupied by dendritic segments. We tackled this question by comparing dendritic length with that of convex hull volume, as it distributes around the cell body. We found that dendritic length and CHP volume distributions were indistinguishable from each other, supporting the conclusion that

466 CHPs are adequate proxies for dendritic distribution at least for our population of tegmental and
467 nigral neurons.
468
469 Overlap between dendritic fields of neighboring neurons is a widely occurring phenomenon in
470 the central nervous system of vertebrates [1–3]. Studying the intersection between dendritic
471 trees of neurons is important for understanding how a neuronal system is organized. For
472 instance, proximity between dendritic trees is an obvious requirement for synaptic dendro-
473 dendritic communication, such as that occurring between olfactory neurons [7] or midbrain
474 dopaminergic neurons themselves [6]. Proximity is also a requirement for dendro-dendritic
475 communication mediated by the dendritic release of neurotransmitters, which are subjected to
476 uptake or degradation following release, as in the case of dendritic dopamine [8] or acetylcholine
477 release from brainstem neurons [33,34], respectively. Evidence also supports the parsimonious
478 idea that dendrites sharing a given locus share the same synaptic inputs (Peters and Feldman,
479 1976, as quoted in [5]). From this argument, it follows that systems in which the dendritic domain
480 of constituent neurons overlap extensively may be characterized by sampling connectivity
481 (archetypical of reticular or brainstem core neurons) and those in which dendritic domains tend
482 to avoid overlap, may be conversely characterized by a selective input strategy (more typical of
483 specific sensory systems) [3,35,36].
484
485 As mentioned, intersection has been mostly studied for neurons in which the receptive field
486 (dendritic or axonal) is two-dimensional, and these studies have focused on determining the
487 average area of receptive fields overlap (or not) with neighboring neurons at the population level

488 using the coverage factor or other meaningful ratios [11]. On the other hand, few studies have
489 examined the geometrical determinants of dendritic fields overlap [37]. We used 3D convex hulls,
490 which for the most part have been used to characterize and classify neuronal populations by CHP
491 shape or size [17–21,38–40], to study dendritic domain intersection between central neurons.
492
493 Our results show that in addition to cell-to-cell distance predictably decreasing intersection,
494 distance versus intersection relationship was not straightforward and had to depend on other
495 geometrical factors. Indeed, intersection was affected by the relative position of each neuron to
496 its pair (i.e. whether one locates besides, above/below, or in front/behind from the other). This
497 is an expected consequence of the dendritic domain of neurons not being spherical (i.e. they are
498 anisotropic) in that maximal extensions in ML, DV or AP axes differ from each other. Indeed, one
499 could argue that differences in intersection curves between tegmental and nigral populations
500 (Fig 11) can be explained by differences in each axes extension (Fig 9B, 10B). The location of the
501 cell body, which we used to identify each neuron "position" and showed ostensible displacement
502 from the dendritic domain's centroid, was also a relevant factor influencing intersection
503 dynamics. Indeed, as seen for the representative example (Fig 8), but also for many neurons in
504 the population (see IR curves for original volume – original shape in Fig 10) intersection ratio was
505 maximal when cell bodies were located some distance apart, not close, from each other. This is
506 an interesting result that challenges the intuitive assumption that neurons whose cell bodies are
507 located next to each other should have a maximal chance of sharing afferents inputs.
508

Perhaps the most remarkable prediction of this study, however, is the finding that dendritic domain intersection is significantly increased by size, and especially shape, homogeneity between neurons (Fig 8, 9 and 10). Or, said conversely, that dendritic domain exclusion between adjacent neurons is significantly increased by heterogeneity in dendritic domain size and shape. The broad spectrum of dendritic domain arrangements among neuronal types has been conceptualized as representing different types of connectivity, either of the selective, sampling or space filling type. The former type is characterized by small dendritic fields occupying a restricted locus, and represents an efficient solution to relay nervous signals from one neuronal stage to another as parallel, separate channels. The sampling strategy (and to some extent the space filling's) connectivity strategy, on the other hand, is characterized by broader dendritic fields encompassing different loci, and represents a solution to increase integration and redundancy in signal transferring [3]. Our results allow us to predict that for systems in which transfer of nervous signal requiring parallel and exclusive transferring of signals may be also accomplished by heterogeneity in both size, but specially shape of dendritic domains.

METHODS

Animals, single neuron labeling and reconstruction

Reconstructed dopaminergic neurons came from a pool of previously reported neurons [14,41,42]. Neurons were labeled with Neurobiotin using juxtacellular or intracellular labeling methods and brain tissue was processed to reveal Neurobiotin and tyrosine hydroxylase to confirm the dopaminergic profile. Next, neurons were manually reconstructed using Neurolucida (MBF Bioscience) from confocal image stacks (more details in Montero et al., 2021). The somatodendritic domain was completely filled, shrinkage corrected and reconstruction tilted-corrected. For some analyses, individual neuronal reconstructions were placed in a custom-made 3D map of substantia nigra and VTA based on [43], according to the ML, DV, and AP location of the cell body.

Shape of CHP

To obtain the actual shape of CHP of an individual neuron, the *convhulln* function in MATLAB was used. The *convhulln* function is based on Quickhull algorithm from Barber et al., 1996, which allows the obtain the smallest CHP from a given set of points. The input for the *convhulln* function was the *Segment points-dendrites* data from Neurolucida, which contains the 3D coordinates of each dendritic segment (S1A Fig, column 1). The outputs of *convhulln* are the list of vertices that form a facet and the volume of the CHP (S1A Fig, column 1). The volumes of CHPs obtained using *convhulln* coincided with the volumes reported for CH by Neurolucida Explorer (MBF Bioscience) (Montero et al., 2021).

Intersected volume methods

Obtaining the volume of the intersected polyhedron required a transformation of the way the CHPs were encoded. For that, we tested 3 methods, which are summarized in S1 Fig. As stated previously, the segment points from a reconstructed neuron were used to obtain the CHP (S1A Fig, column 1). For method 1, we added a 3D grid of points using the *ndgrid* function of MATLAB (1 µm distance between points) to a cuboid formed by the maximal ML, DV, and AP extensions of the neuron CHP (S1A Fig, column 2) and, using the *inhull* function (D'Errico 2021, S1A Fig, column 3), obtained the 3D grid of points that located inside the CHP. We confirmed that the obtained volume corresponded to the original measured volume using the *convhulln* function. For method 2, we added the same 3D grid of points using the *ndgrid* function of method 1, but instead of selecting those points inside the hull, we selected only those points from the 3D grid that were in touch with the CHP facets (S1A Fig, column 3). Again, we confirmed that the obtained volume corresponded to the *convhulln* function volume. For method 3, we started from the original CHP and obtained the vertices (S1A Fig, columns 1 and 2). By using the *linspace* function, vertices forming each CHP facet were joined using 1000 points per CHP edge (S1A Fig, column 3). Thus, we ended with three transformed CHP defined by either: (1) points filling the CHP volume, (2) points covering the CHP facets and (3) points lined up along edges. These three different ways of encoding CHPs were tested for finding the intersected polyhedron volume between a pair of CHPs

566 Using method 1 (points filling the CHP), for a given pair of CHP points, the common points
567 between the pair of CHPS were obtained using the *intersect* function. Intersected points were
568 then used to obtain a CHP using *convhulln*, and the intersected volume in mm^3 was obtained (S1B
569 Fig, first row). For method 2 (points covering facets), the points of each CHP facet that are inside
570 the other CHP were found using the *inhull* function. Again, with these outputs of points, the
571 intersected CHP can be calculated using *convhulln* and the intersected volume measured (S1B
572 Fig, second row). With method 3 (points lining up edges), the procedure is similar to method 2:
573 using the *inhull* function, the points from each CHP edge that are inside the other CHP of the pair
574 are obtained, and then the *convhulln* function is used to obtain the intersected CHP and the
575 intersected volume (S1B Fig, third row). While all three methods allowed to obtain a similar
576 intersected volume, big differences were found regarding the time required to complete the
577 intersection calculation. Using a sample of 15 SNc dopaminergic neurons and testing all the
578 possible pairs without repeating reciprocal distances (105 pairs of CHPs in total), method 1
579 showed a mean calculation time per pair of CHP of 68.18 $\pm$ 3.51 sec, followed by method 2, with
580 9.06 $\pm$ 0.38 sec. Method 3 was the fastest of the three methods, with a mean calculation time of
581 0.21 $\pm$ 0.01 sec. Considering that method 3 was the fastest without losing accuracy, this method
582 was used in all the following analyses.
583
584

585 **Wedge Analysis**

586 We used the 3D wedge function from Neurolucida Explorer software. In this analysis, the
587 distribution of the processes as they extend from the centroid of the cell body in every direction

588 is obtained. To achieve this, the neuron is placed in the center of a cylinder, which in this study
589 was divided into 4 angular wedges, and in 2 parallel planes perpendicular to the direction of the
590 cylinder, with the division of the planes centered in the cell body. For instance, if the cylinder is
591 placed parallel to the anteroposterior axis, the four angular wedges report the location of the
592 processes in the dorsomedial, ventromedial, ventrolateral, and dorsolateral quadrants, at each
593 of the 2 planes defined in the AP axis (Fig 2A1, S4A Fig). Results were presented as a percentage
594 of the total dendritic length in each quadrant. A similar procedure was used to analyze the wedge
595 from CHPs (CHP wedge analysis, Fig 2A2, S4A Fig). This analysis was performed using a custom
596 MATLAB script. In this case, the percentage of the total CHP volume was determined in each
597 quadrant of the anterior and posterior planes. A further CHP wedge analysis was carried out for
598 SNc and VTA average CHP shapes (explained above).
599
600 **Intersecting ratio**. It was reasoned that because the intersected volume depends strongly on the
601 volume of individual CHP neurons (for instance, the intersected volume of two large but
602 minimally intersected neurons could be the same as the intersected volume of two small but
603 largely intersected neurons), it was necessary to find a ratio that normalized for the volume. As
604 such it was decided to work with an intersection ratio (IR), that is defined as follows:

605 $$Intersection\ Ratio = \frac{Intersected\ Volume}{Non_intersected\ Volume} x\ 100$$

606 $$Non\text{-}intersected\ Volume = CHP\ Volume\ 1 + CHP\ Volume\ 2 - Intersected\ Volume$$

607 For example, the pair of CHPs in S5A Fig exhibit a larger intersected volume than the pair of CHPs
608 in S5B Fig, but when each intersected volume is divided by their corresponding non-intersected
609 volume, the IR is comparable between these two pairs of CHPs. We decided to normalize by the

610 non-intersected volume, and not by the total added volume of both individual neurons, so that
611 the ratio approaches 100 (and not 50), for maximally overlapping CHP. In any event, the results
612 in the vast majority of analysis did not vary between ratios using either the *non-intersected*
613 *volume* or the *total added volume* as divisors (not shown), nor when total intersected volume
614 was used.
615

616 Method for change CHP volume

617 Using a custom MATLAB script, CHP volume can be modified by multiplying the CHPs vertices
618 coordinates by the following conversion factor:

619 $$\sqrt[3]{\frac{New\ CHP\ volume}{Original\ CHP\ volume}}$$

620 The converted CHPs conserve their shape and the position of their cell body. We used this
621 procedure to change the analyzed sample of neurons to a new CHP volume that corresponded
622 to the average between the CHP volumes of a pair of neurons (Figs 5 and 7), the average of
623 tegmental (Fig 9) or nigral (Fig 10) neurons, and the average of tegmental + nigral (Fig 11)
624 neurons.
625
626
627

628 Method for determining CHP average shape

629 To address the effect of CHP shape on IR, we needed first a rationale and then a method to define
630 an average CHP in 3D. The chosen rationale can be narrated as follows: let's imagine an apex

631 centered at 0, 0, 0 and from which rays emanate in all directions in space. Then the somatic
632 centers of a pair of CHP are placed at the apex (as shown in Fig 6, see also S3 Fig). Any single ray
633 will intersect the facets of the two CHP at distances d1 and d2. Then, a point at mid-distance
634 between d1 and d2 is defined, and the exercise is repeated for all rays emanating from the apex.
635 A new polyhedron will be created by all points located at mid-distance between the facets of
636 both CHP at every solid angle. This procedure can be projected to a larger number of CHP
637 neurons, in which case the points of the new polyhedron will correspond to the average of all *n*
638 distances at which rays intersect the facets of all CHP in a given ray direction.
639
640 Explained in detail, the procedure is based on a surface-to-point transformation procedure. It
641 starts placing the somatic center of a CHP on the center of a Cartesian space (0, 0, 0) where the
642 three orthogonal axes (ML, DV and AP) intersect. Then, a plane (e.g. AP – ML plane) orthogonal
643 to one axis (DV) is chosen, and the distances from the center to the CHP facets in that plane are
644 measured. This is repeated 360 times in 1-degree steps, in an anticlockwise direction. That
645 defines a polygon formed by 360 points (S3 A1-5 Fig). To move from that polygon to a 3D
646 polyhedron, the original plane is systematically tilted in 1-degree steps around a new axis (e.g.
647 the ML axis). That creates a polyhedron with 64800 points on its surface (S3 A6-10 Fig). To obtain
648 a CHP average from a given number of CHPs, the transformed CHPs were centered in the origin,
649 using the somatic center as a reference point. Then, the mid-distance between analogous points
650 on the surface of their respective CHP was determined. A simplified 2D explanation for the
651 average process of 2 or 15 convex hull polygons is provided in S3A and B Figs, respectively. It
652 should be noticed that a consequence of this procedure is that the resulting polyhedron (or

resulting polygon in the simplified 2D explanation of S3A and B Figs)) is likely not to be convex all around its surface (S3A Fig), for which an approximate convex hull must be defined using the *convhulln* function. On the other hand, the more CHP are included, the more similar is the resulting polyhedron to its convex hull (S3B Fig).

Computational and statistical analysis

MATLAB R2018a was used on a Lenovo P51 (Intel i7-7820HQ, 16 Gb of RAM, NVIDIA Quadro M1200) with Windows 10. Statistical analyses were performed on MATLAB. Two-way ANOVA was used (Fig 2B, S4A Fig). Friedman test followed by Dunn-Sidak post-test and Wilcoxon rank sum test were performed (Figs 9-11). An exponential decay model was used when required (Fig 11D). Significance for all statistical tests was set at $p < 0.05$.

Acknowledgments

We thank Luciana López-Juri for her insightful comments during the progress of this work.

668 # References

669 1. Nieuwenhuys R, Donkelaar HJ, Nicholson C. The Central Nervous System of Vertebrates:
670 With Posters. Springer; 1998.
671 2. Cajal SR. Textura del sistema nervioso del hombre y de los vertebrados: estudios sobre el
672 plan estructural y composición histológica de los centros nerviosos adicionados de
673 consideraciones fisiológicas fundadas en los nuevos descubrimientos. N. Moya; 1904.
674 3. Harris KM, Spacek J. Chapter 1: Dendrite structure; in Dendrites. 3th ed. Stuart G,
675 Spruston N, Häusser M, editors. OUP Oxford; 2017.
676 4. Peters A, Feldman ML. The projection of the lateral geniculate nucleus to area 17 of the
677 rat cerebral cortex. I. General description. J Neurocytol. 1976;5: 63–84.
678 doi:10.1007/BF01176183
679 5. Packer AM, McConnell DJ, Fino E, Yuste R. Axo-dendritic overlap and laminar projection
680 can explain interneuron connectivity to pyramidal cells. Cereb Cortex. 2013;23: 2790–
681 2802. doi:10.1093/cercor/bhs210
682 6. Groves PM, Linder JC. Dendro-dendritic synapses in substantia nigra: Descriptions based
683 on analysis of serial sections. Exp Brain Res. 1983;49: 209–217. doi:10.1007/BF00238581
684 7. Hinds JW. Reciprocal and serial dendrodendritic synapses in the glomerular layer of the
685 rat olfactory bulb. Brain Res. 1970;17: 530–534. doi:10.1016/0006-8993(70)90263-5
686 8. Rice ME, Patel JC. Somatodendritic dopamine release: Recent mechanistic insights. Philos
687 Trans R Soc B Biol Sci. 2015;370: 1–14. doi:10.1098/rstb.2014.0185
688 9. Jan YN, Jan LY. Branching out: Mechanisms of dendritic arborization. Nature Reviews
689 Neuroscience. 2010. pp. 316–328. doi:10.1038/nrn2836

690 10. Farajian R, Raven MA, Cusato K, Reese BE. Cellular positioning and dendritic field size of
691 cholinergic amacrine cells are impervious to early ablation of neighboring cells in the
692 mouse retina. Vis Neurosci. 2004;21: 13–22. doi:10.1017/S0952523804041021
693 11. Lefebvre JL, Sanes JR, Kay JN. Development of Dendritic Form and Function. Annu Rev
694 Cell Dev Biol. 2015;31: 741–777. doi:10.1146/annurev-cellbio-100913-013020
695 12. Grueber WB, Sagasti A. Self-avoidance and tiling: Mechanisms of dendrite and axon
696 spacing. Cold Spring Harbor perspectives in biology. 2010. pp. 1–16.
697 doi:10.1101/cshperspect.a001750
698 13. Dacey DM, Petersen MR. Dendritic field size and morphology of midget and parasol
699 ganglion cells of the human retina. Proc Natl Acad Sci U S A. 1992;89: 9666–9670.
700 doi:10.1073/pnas.89.20.9666
701 14. Montero T, Gatica RI, Farassat N, Meza R, González-Cabrera C, Roeper J, et al. Dendritic
702 Architecture Predicts in vivo Firing Pattern in Mouse Ventral Tegmental Area and
703 Substantia Nigra Dopaminergic Neurons. Front Neural Circuits. 2021;15: 1–16.
704 doi:10.3389/fncir.2021.769342
705 15. Henny P, Brown MTC, Northrop A, Faunes M, Ungless M a, Magill PJ, et al. Structural
706 correlates of heterogeneous in vivo activity of midbrain dopaminergic neurons. Nat
707 Neurosci. 2012;15: 613–619. doi:10.1038/nn.3048
708 16. Vrieler N, Loyola S, Yarden-Rabinowitz Y, Hoogendorp J, Medvedev N, Hoogland TM, et
709 al. Variability and directionality of inferior olive neuron dendrites revealed by detailed 3D
710 characterization of an extensive morphological library. Brain Struct Funct. 2019;224:
711 1677–1695. doi:10.1007/s00429-019-01859-z

17. Malmierca MS, Seip KL, Osen KK. Morphological classification and identification of neurons in the inferior colliculus: a multivariate analysis. Anat Embryol (Berl). 1995;191: 343–350. doi:10.1007/BF00534687

18. Gärtner U, Alpár A, Reimann F, Seeger G, Heumann R, Arendt T. Constitutive Ras activity induces hippocampal hypertrophy and remodeling of pyramidal neurons in synRas mice. J Neurosci Res. 2004;77: 630–641. doi:10.1002/jnr.20194

19. Gertler TS, Chan CS, Surmeier DJ. Dichotomous anatomical properties of adult striatal medium spiny neurons. J Neurosci. 2008;28: 10814–10824. doi:10.1523/JNEUROSCI.2660-08.2008

20. Felix RA, Vonderschen K, Berrebi AS, Magnusson AK. Development of on-off spiking in superior paraolivary nucleus neurons of the mouse. J Neurophysiol. 2013;109: 2691–2704. doi:10.1152/jn.01041.2012

21. Ito T. Different coding strategy of sound information between GABAergic and glutamatergic neurons in the auditory midbrain. J Physiol. 2020;598: 1039–1072. doi:10.1113/JP279296

22. Chazelle B, Dobkin DP. Intersection of convex objects in two and three dimensions. J ACM. 1987;34: 1–27. doi:10.1145/7531.24036

23. O'Rourke J, Chien C Bin, Olson T, Naddor D. A new linear algorithm for intersecting convex polygons. Comput Graph Image Process. 1982;19: 384–391. doi:10.1016/0146-664X(82)90023-5

24. Muller DE, Preparata FP. Finding the intersection of two convex polyhedra. Theor Comput Sci. 1978;7: 217–236. doi:https://doi.org/10.1016/0304-3975(78)90051-8

25. Govender N, Rajamani R, Wilke DN, Wu CY, Khinast J, Glasser BJ. Effect of particle shape in grinding mills using a GPU based DEM code. Miner Eng. 2018;129: 71–84. doi:10.1016/j.mineng.2018.09.019

26. Marks WB, Burke RE. Simulation of motoneuron morphology in three dimensions. II. Building complete neurons. J Comp Neurol. 2007;503: 701–716. doi:10.1002/cne.21417

27. Nedelescu H, Abdelhack M, Pritchard AT. Regional differences in Purkinje cell morphology in the cerebellar vermis of male mice. J Neurosci Res. 2018;96: 1476–1489. doi:10.1002/jnr.24206

28. Gregory AD, State A, Lin MC, Manocha D, Livingston MA. Feature-based surface decomposition for polyhedral morphing. Proc Annu Symp Comput Geom. 1999; 415–416. doi:10.1145/304893.304998

29. Kang JY, Lee BS. Mesh-based morphing method for rapid hull form generation. CAD Comput Aided Des. 2010;42: 970–976. doi:10.1016/j.cad.2009.07.001

30. Huang YJ, Lin WC, Yeh IC, Lee TY. Geometric and Textural Blending for 3D Model Stylization. IEEE Trans Vis Comput Graph. 2018;24: 1114–1126. doi:10.1109/TVCG.2017.2657751

31. Erikson C. Morphing Three Dimensional Polyhedral Objects. Honor Pap. 1994.

32. Alexa M. Recent advances in mesh morphing. Comput Graph Forum. 2002;21: 173–198. doi:10.1111/1467-8659.00575

33. Garzón M, Pickel VM. Dendritic and axonal targeting of the vesicular acetylcholine transporter to membranous cytoplasmic organelles in laterodorsal and pedunculopontine tegmental nuclei. J Comp Neurol. 2000;419: 32–48.

doi:10.1002/(SICI)1096-9861(20000327)419:1<32::AID-CNE2>3.0.CO;2-O

34. Garzón M, Pickel VM. Electron microscopic localization of M2-muscarinic receptors in cholinergic and noncholinergic neurons of the laterodorsal tegmental and pedunculopontine nuclei of the rat mesopontine tegmentum. J Comp Neurol. 2016;524: 3084–3103. doi:https://doi.org/10.1002/cne.24010

35. Ramón-Moliner E, Nauta WJH. The isodendritic core of the brain stem. J Comp Neurol. 1966;126: 311–335. doi:10.1002/cne.901260301

36. Geisler S, Zahm DS. Afferents of the ventral tegmental area in the rat-anatomical substratum for integrative functions. J Comp Neurol. 2005;490: 270–294. doi:10.1002/cne.20668

37. Wässle H, Peichl L, Boycott BB. Dendritic territories of cat retinal ganglion cells. Nature. 1981;292: 344–345. doi:10.1038/292344a0

38. Mihaljević B, Benavides-Piccione R, Bielza C, DeFelipe J, Larrañaga P. Bayesian Network Classifiers for Categorizing Cortical GABAergic Interneurons. Neuroinformatics. 2015;13: 193–208. doi:10.1007/s12021-014-9254-1

39. Kawa A, Stahlhut M, Berezin A, Bock E, Berezin V. A simple procedure for morphometric analysis of processes and growth cones of neurons in culture using parameters derived from the contour and convex hull of the object. J Neurosci Methods. 1998;79: 53–64. doi:10.1016/S0165-0270(97)00165-9

40. Rojo C, Leguey I, Kastanauskaite A, Bielza C, Larrañaga P, Defelipe J, et al. Laminar Differences in Dendritic Structure of Pyramidal Neurons in the Juvenile Rat Somatosensory Cortex. Cereb Cortex. 2016;26: 2811–2822. doi:10.1093/cercor/bhv316

41. Meza RC, López-Jury L, Canavier CC, Henny P. Role of the axon initial segment in the control of spontaneous frequency of nigral dopaminergic neurons in vivo. J Neurosci. 2018;38: 733–744. doi:10.1523/JNEUROSCI.1432-17.2017

42. Farassat N, Costa KM, Stojanovic S, Albert S, Kovacheva L, Shin J, et al. In vivo functional diversity of midbrain dopamine neurons within identified axonal projections. Elife. 2019;8. doi:10.7554/eLife.48408

43. Fu YH, Yuan Y, Halliday G, Rusznák Z, Watson C, Paxinos G. A cytoarchitectonic and chemoarchitectonic analysis of the dopamine cell groups in the substantia nigra, ventral tegmental area, and retrorubral field in the mouse. Brain Struct Funct. 2012;217: 591–612. doi:10.1007/s00429-011-0349-2

44. Barber CB, Dobkin DP, Huhdanpaa H. The Quickhull Algorithm for Convex Hulls. ACM Trans Math Softw. 1996;22: 469–483. doi:10.1145/235815.235821

45. D'Errico J. Inhull. 2021 [cited 14 Jun 2021]. Available: https://www.mathworks.com/matlabcentral/fileexchange/10226-inhull

794 **S1 Fig. Methods to quantify the intersected volume between CHPs.** A) CHP transformation
795 methods. We started using the dendritic segment points from a digitally reconstructed neuron
796 (blue points, top left diagram). The cell body is represented with a disc. Then, the CHP from the
797 neuron was obtained (blue lines, middle left diagram). Following, a grid of points was generated
798 around the CHP (red points), on a grid equal to the maximal extension of the CHP in the ML, DV
799 and AP axis (middle center diagram). Grid points separation = 1 µm. Next, the points of the grid
800 that were inside of the CHP were determined (blue points, top center diagram). For method 1,
801 the points located inside the CHP were used (top right diagram). For method 2, the points from
802 the grid that were touching the CHP facets were used (middle right diagram). For method 3, the
803 vertices from the CHP (blue open circles, bottom center diagram), were used to define the CHP
804 edges linking the CHP vertices using points (1000 points per edge, bottom right diagram). B) CHP
805 intersection quantification methods. A pair of CHPs was tested to obtain the intersected volume
806 using the transformed CHP with the three methods described in (A). With method 1, the
807 intersected points from each grid of CHPs were obtained. Using method 2, the points from the
808 surface of the first CHP that were inside the second CHP were obtained, and conversely the points
809 from the surface of the second CHP that were inside the first CHP were obtained. For method 3,
810 the points from the edges of the first CHP that were inside the second CHP were obtained, and
811 conversely the points from the edges of the second CHP that were inside the first CHP were
812 obtained. The calculated intersected volume for each method was similar (Method 1= 0.024
813 mm^3; Method 2= 0.025 mm^3; Method 3= 0.024 mm^3). However, differences were found in the
814 time spent to calculate the intersection (for a sample of 105 pairs of SNc CHPs, Method 1 = 68.18
815 $\pm$ 3.51 sec; Method 2 = 9.06 $\pm$ 0.38 sec; Method 3= 0.21 $\pm$ 0.01 sec).

816 **S2 Fig. Intersected volume from a sample of CHP from SNc and VTA dopaminergic neurons.**
817 Measurement of the intersected volume between pairs of CHPs from SNc (A) and VTA (B), as
818 measured in their corresponding position in each area. A total of 105 pairs of CHPs were tested
819 in each area. Each point represents the intersected volume value of a pair of CHPs.
820 **S3 Fig. Simplified 2D representation of average shape computation.** A) Average shape method
821 explained for a pair of 2D CH polygons. The polygons were centered in the origin in relation to
822 their cell body, and a line is plotted at 0 degrees. The average point from the sample of 2 points
823 in the given angle was obtained (black open circle, A1). Next, the process was repeated at 1-
824 degree steps (A2-A5). Finally, 360 points were obtained, that were transformed to the average
825 CHP shape using the *convhulln* function (A6). B) Average shape method explained for a group of
826 15 2D polygons. CHPs were centered in the origin (B1) and the average of the points in each angle
827 were obtained (B2). Then, the average CHP shape was calculated using the *convhulln* function
828 (B3). Scaling is different for examples B and C.
829 **S4 Fig. IR variability from a sample of nigral neurons.** A) Distribution of dendritic trees and CHPs
830 volume for nigral neurons (n = 15 neurons). When a repeated measures two-way ANOVA was
831 performed within planes and within dendritc length and CHP volume wedge, no significant
832 differences were found: Interaction, $F_{(3,42)}$= 0.2566, p=0.8562 (A1); $F_{(3,42)}$= 0.9138, p=0.4425 (A2).
833 B) Representative examples of nigral neurons and their CHPs, as observed from the frontal,
834 lateral and dorsal view. At a similar distance between cell bodies, CHP pair A shows a much higher
835 IR than CHP pairs B. These examples are highlighted in figure B (red points and letters). Gray
836 volume represents intersected volume. Cell bodies are represented with solid circles. C)
837 Measurement of the IR between pairs of CHP from SNc, as measured in their corresponding

838 position in each area. Each point represents the IR value of a pair of CHPs.

839 **S5 Fig. Using IR to normalize the intersected volume between pairs of CHPs**. Two examples of

840 CHP intersection are shown (A1-A2). The pairs of neurons show a different intersected volume,

841 but a similar IR. Gray volume represents intersected volume.

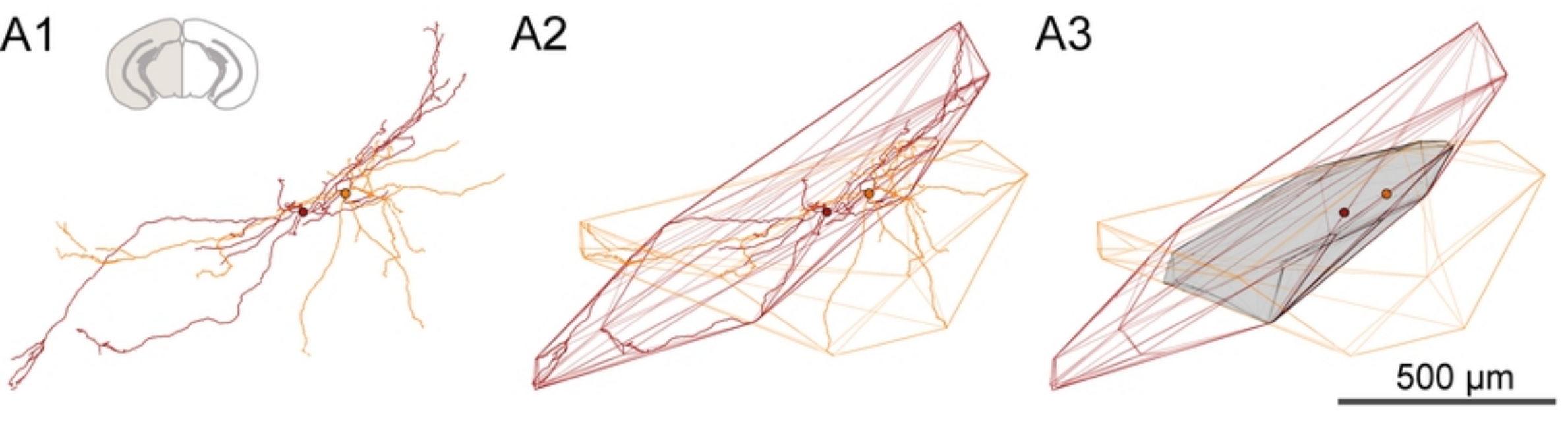

Fig 1

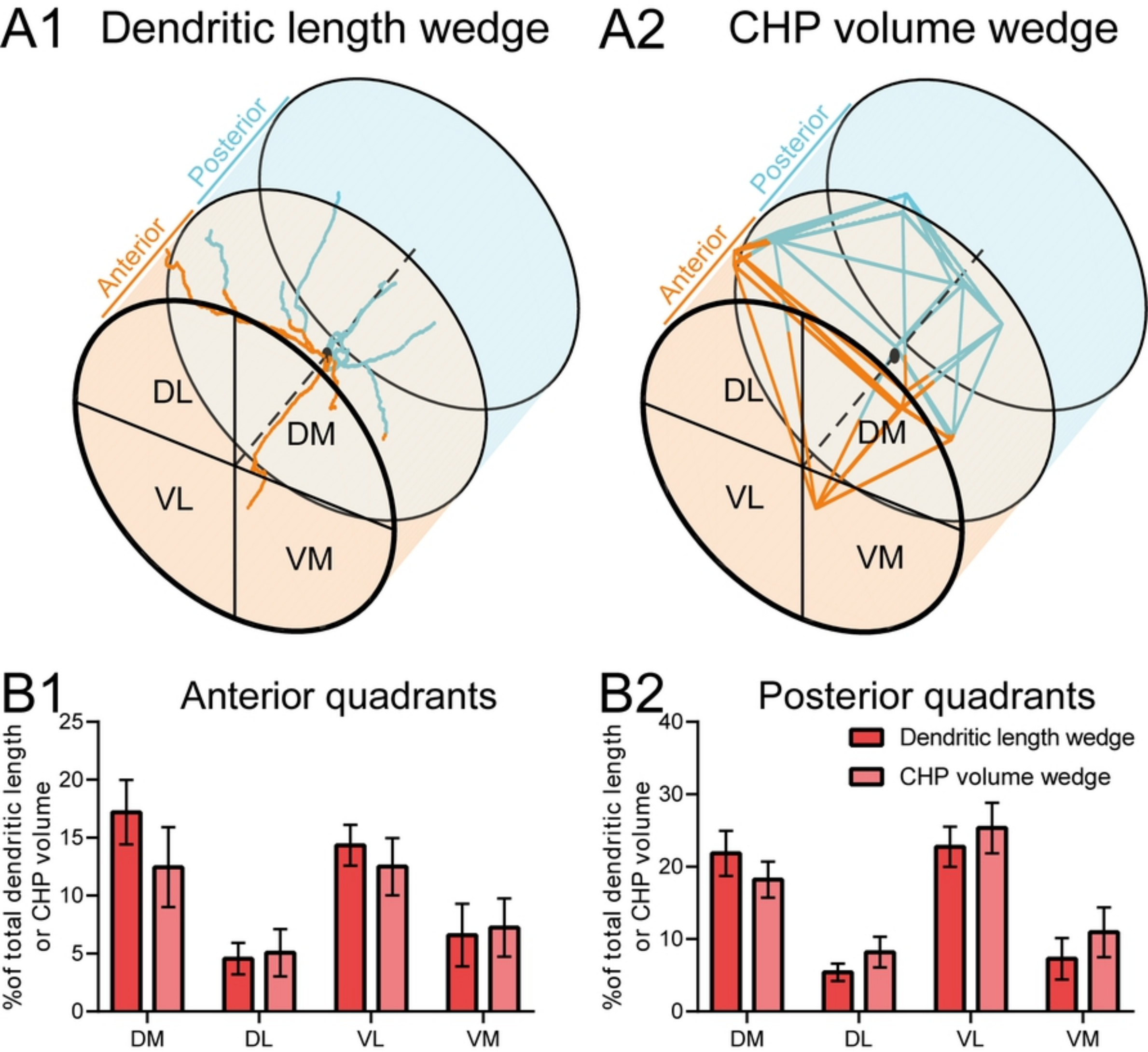
A1
Dendritic length wedge
Posterior
Anterior
DL
DM
VL
VM
A2
CHP volume wedge
Posterior
Anterior
DL
DM
VL
VM
B1
Anterior quadrants
%of total dendritic length or CHP volume
25
20
15
10
5
0
DM
DL
VL
VM
B2
Posterior quadrants
Dendritic length wedge
CHP volume wedge
%of total dendritic length or CHP volume
40
30
20
10
0
DM
DL
VL
VM

Fig 2

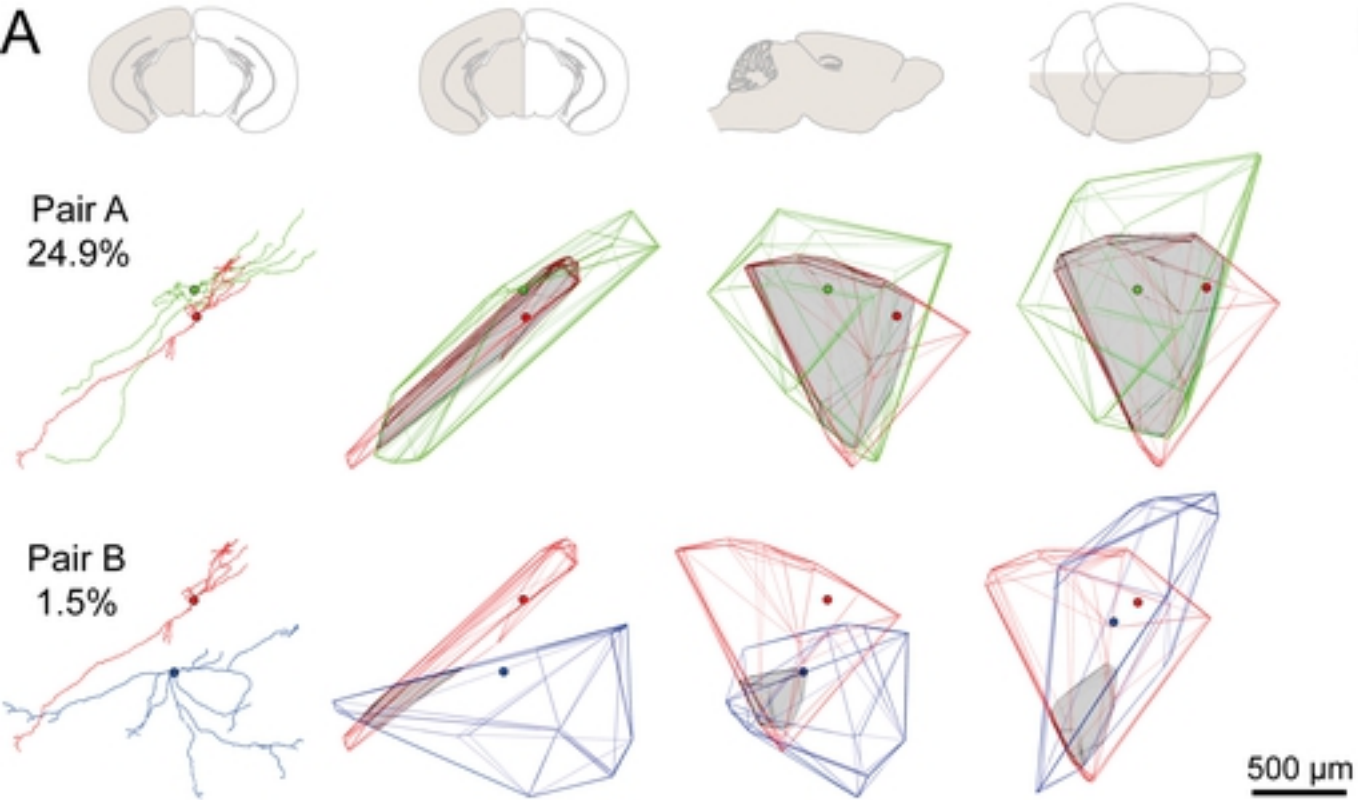
A
Pair A
24.9%
Pair B
1.5%
500 µm

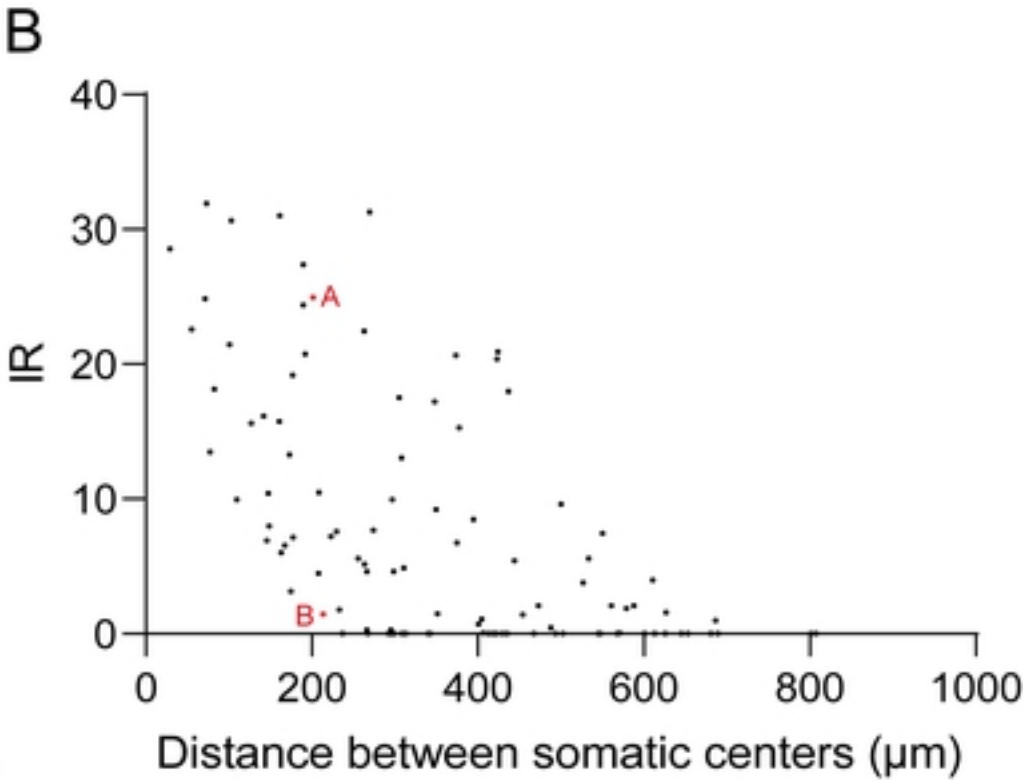
B
IR
40
30
20
10
0
A
B
0
200
400
600
800
1000
Distance between somatic centers (µm)

Fig 3

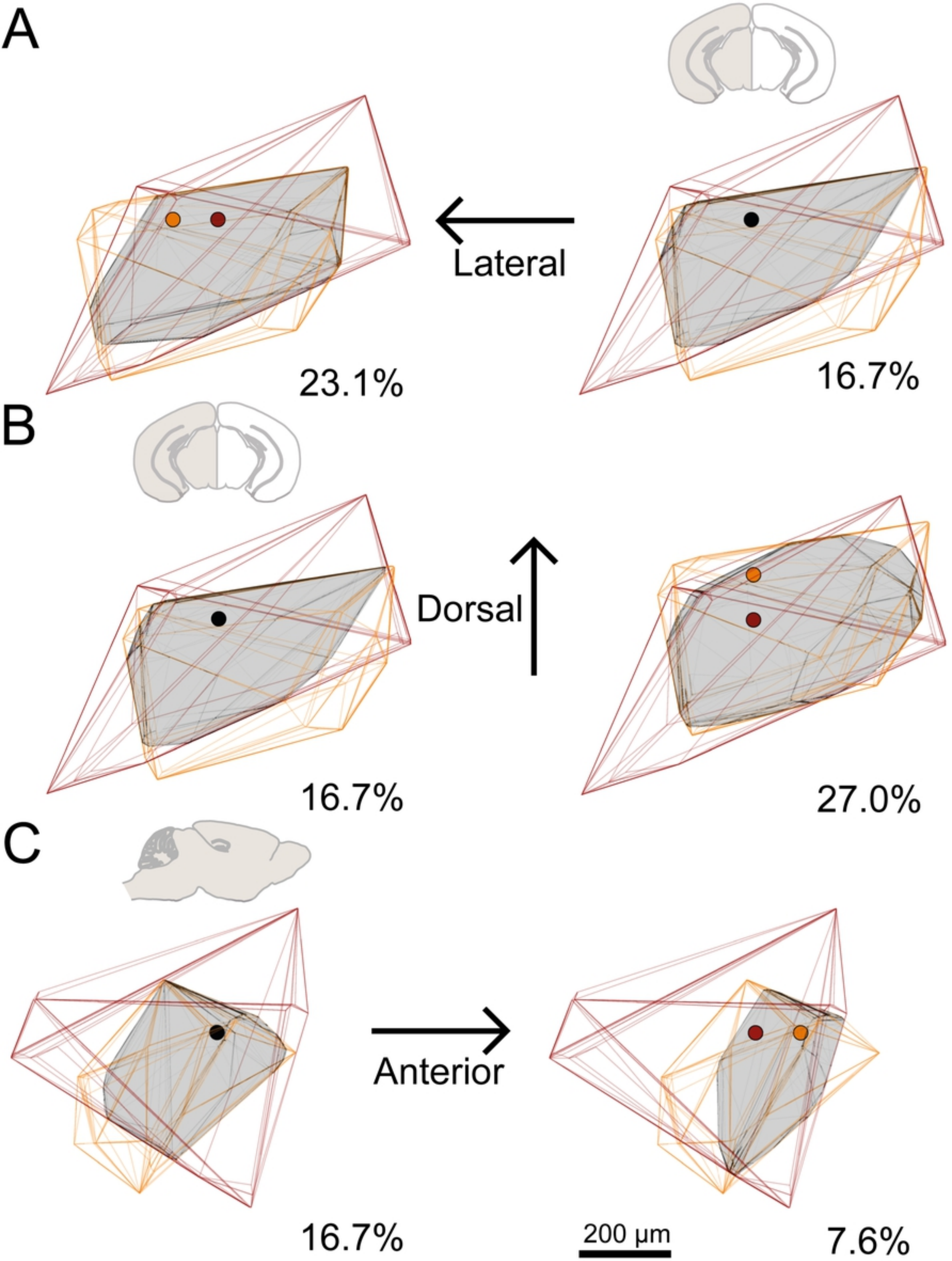

Fig 4

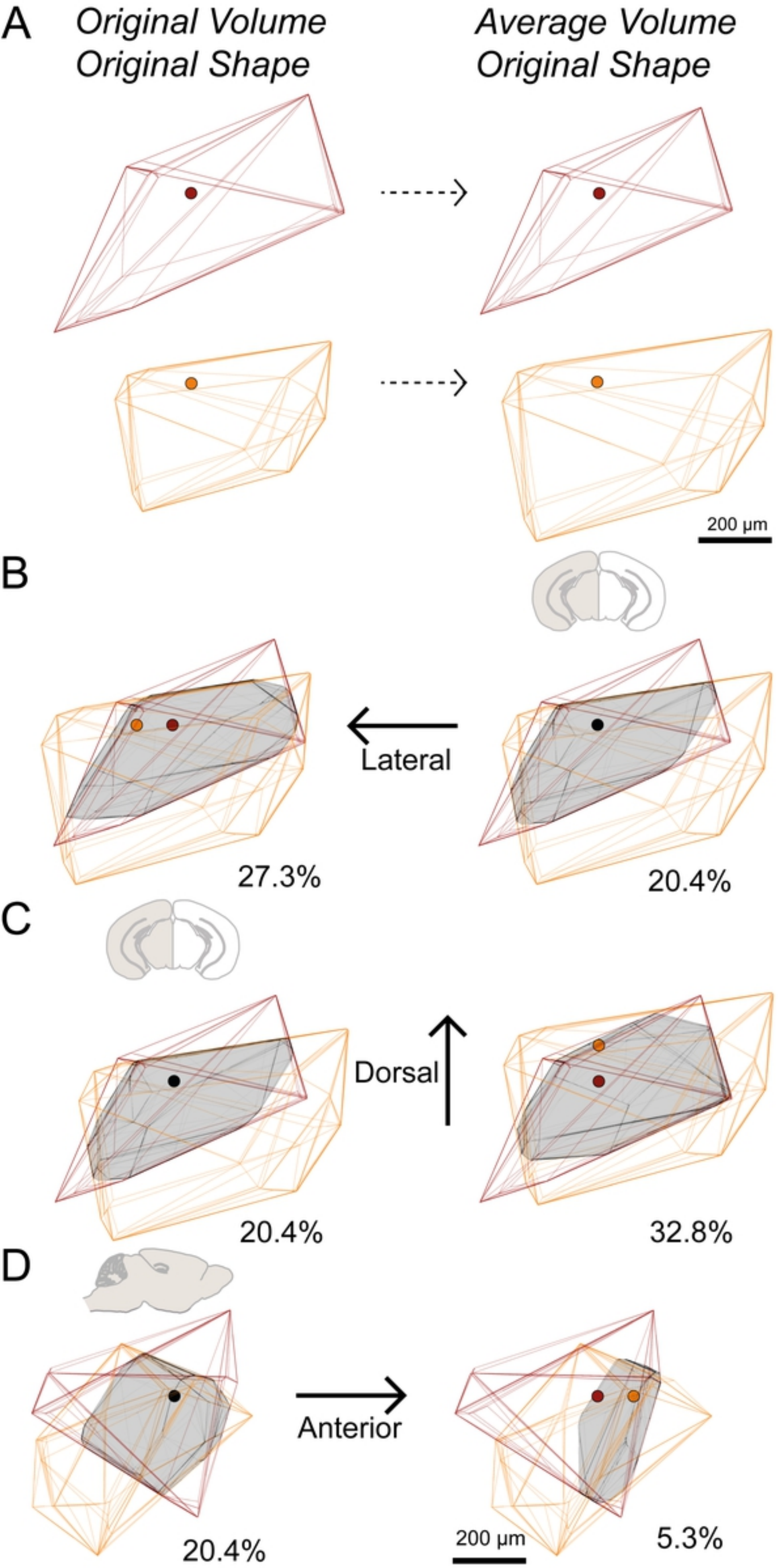
A
Original Volume
Original Shape
Average Volume
Original Shape
200 µm
B
Lateral
27.3%
20.4%
C
Dorsal
20.4%
32.8%
D
Anterior
20.4%
200 µm
5.3%

Fig 5

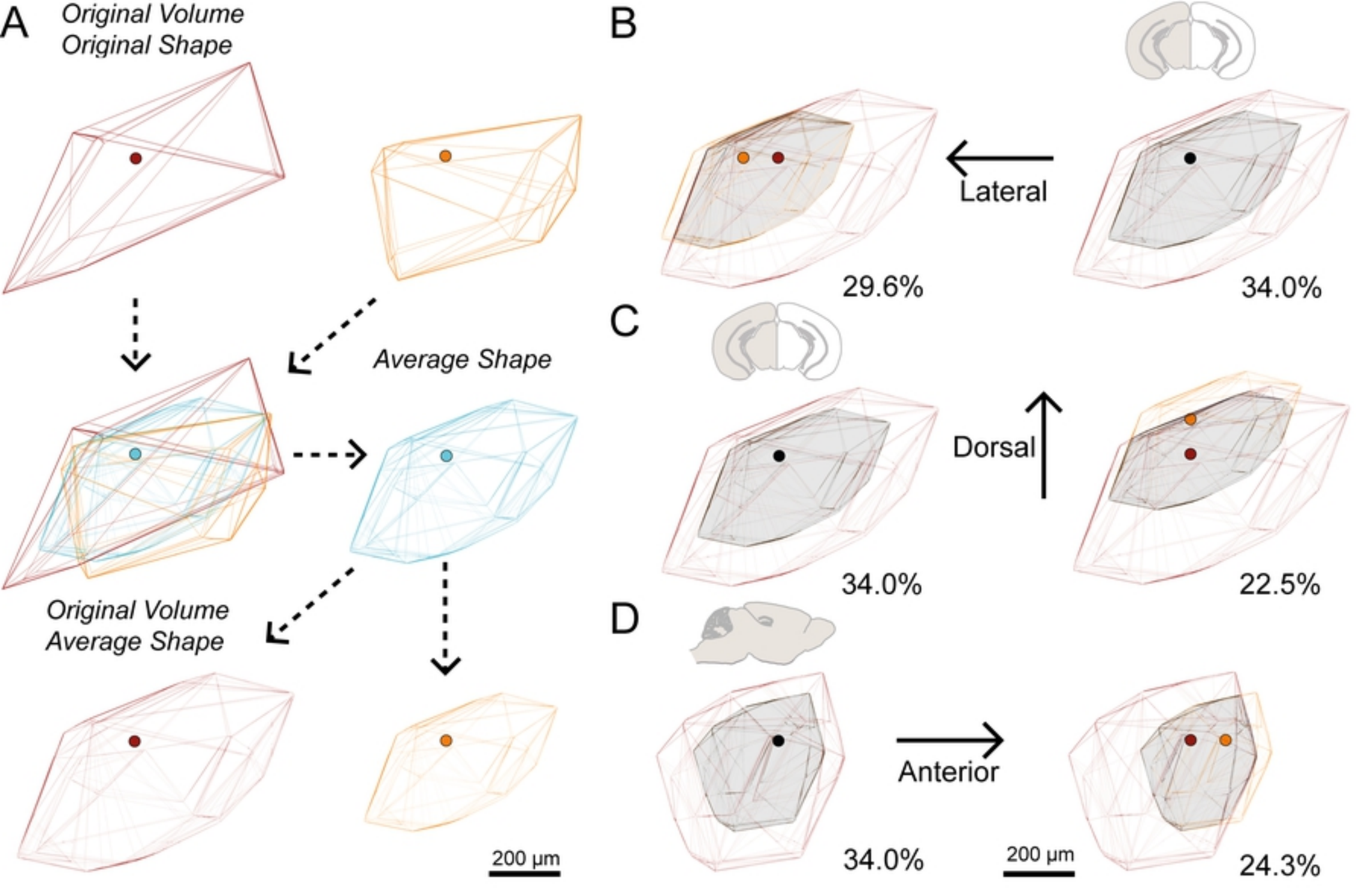
A
Original Volume
Original Shape
Average Shape
Original Volume
Average Shape
200 µm
B
Lateral
29.6%
34.0%
C
Dorsal
34.0%
22.5%
D
Anterior
34.0%
200 µm
24.3%

Fig 6

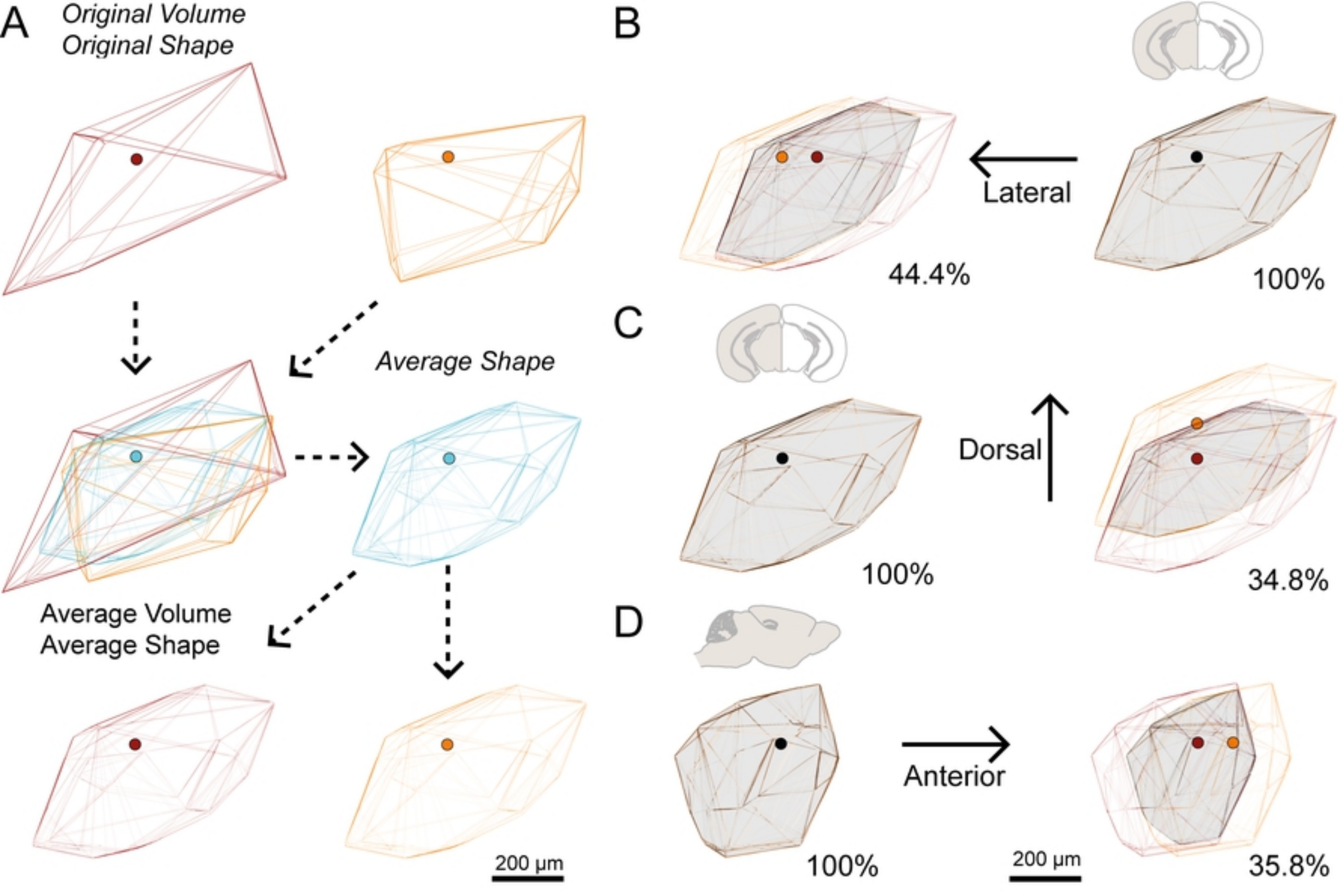
A
Original Volume
Original Shape
Average Shape
Average Volume
Average Shape
200 µm
B
Lateral
44.4%
100%
C
Dorsal
100%
34.8%
D
Anterior
100%
200 µm
35.8%

Fig 7

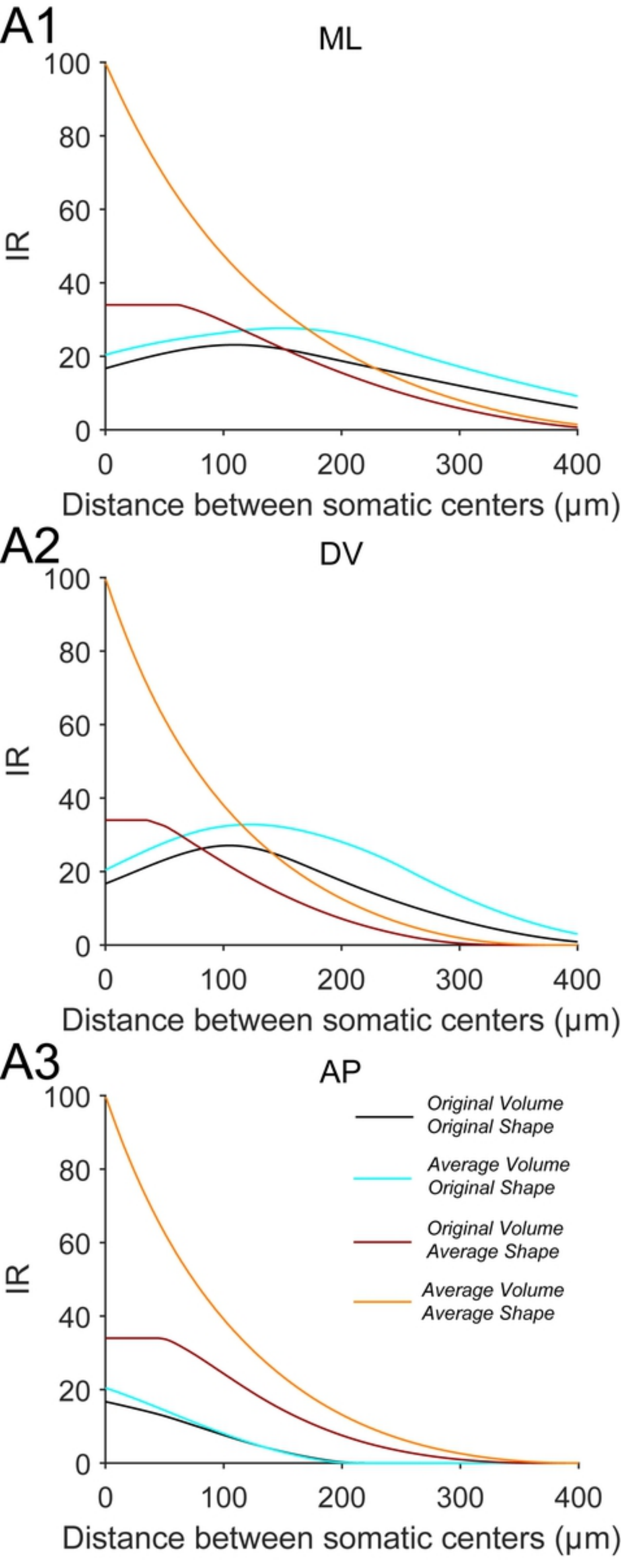
A1
ML
IR
100
80
60
40
20
0
0
100
200
300
400
Distance between somatic centers (μm)
A2
DV
IR
100
80
60
40
20
0
0
100
200
300
400
Distance between somatic centers (μm)
A3
AP
IR
100
80
60
40
20
0
0
100
200
300
400
Distance between somatic centers (μm)
Original Volume
Original Shape
Average Volume
Original Shape
Original Volume
Average Shape
Average Volume
Average Shape

Fig 8

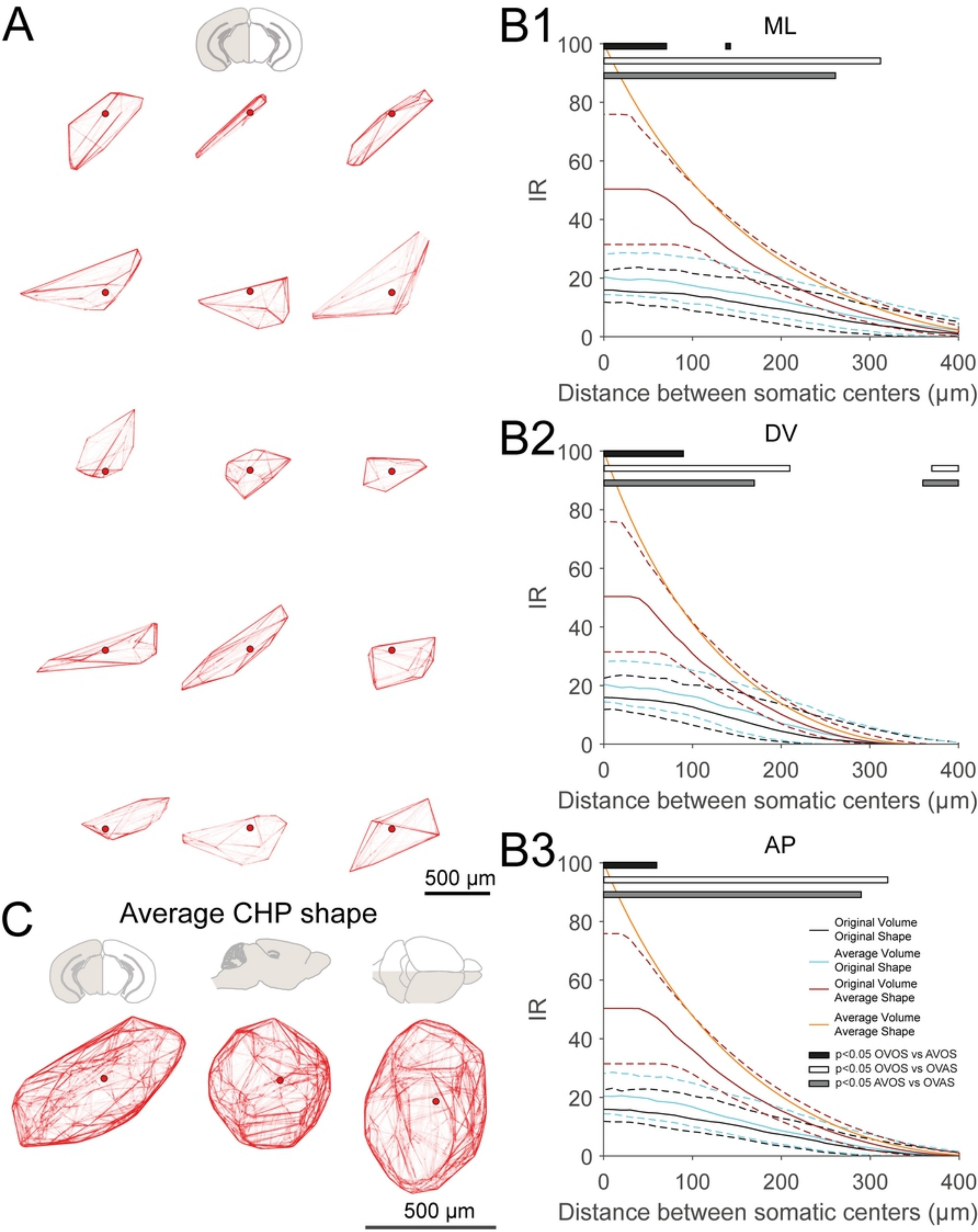
A
B1
ML
B2
DV
B3
AP
IR
Distance between somatic centers (μm)
Original Volume Original Shape
Average Volume Original Shape
Original Volume Average Shape
Average Volume Average Shape
p<0.05 OVOS vs AVOS
p<0.05 OVOS vs OVAS
p<0.05 AVOS vs OVAS
500 μm
C
Average CHP shape
500 μm

Fig 9

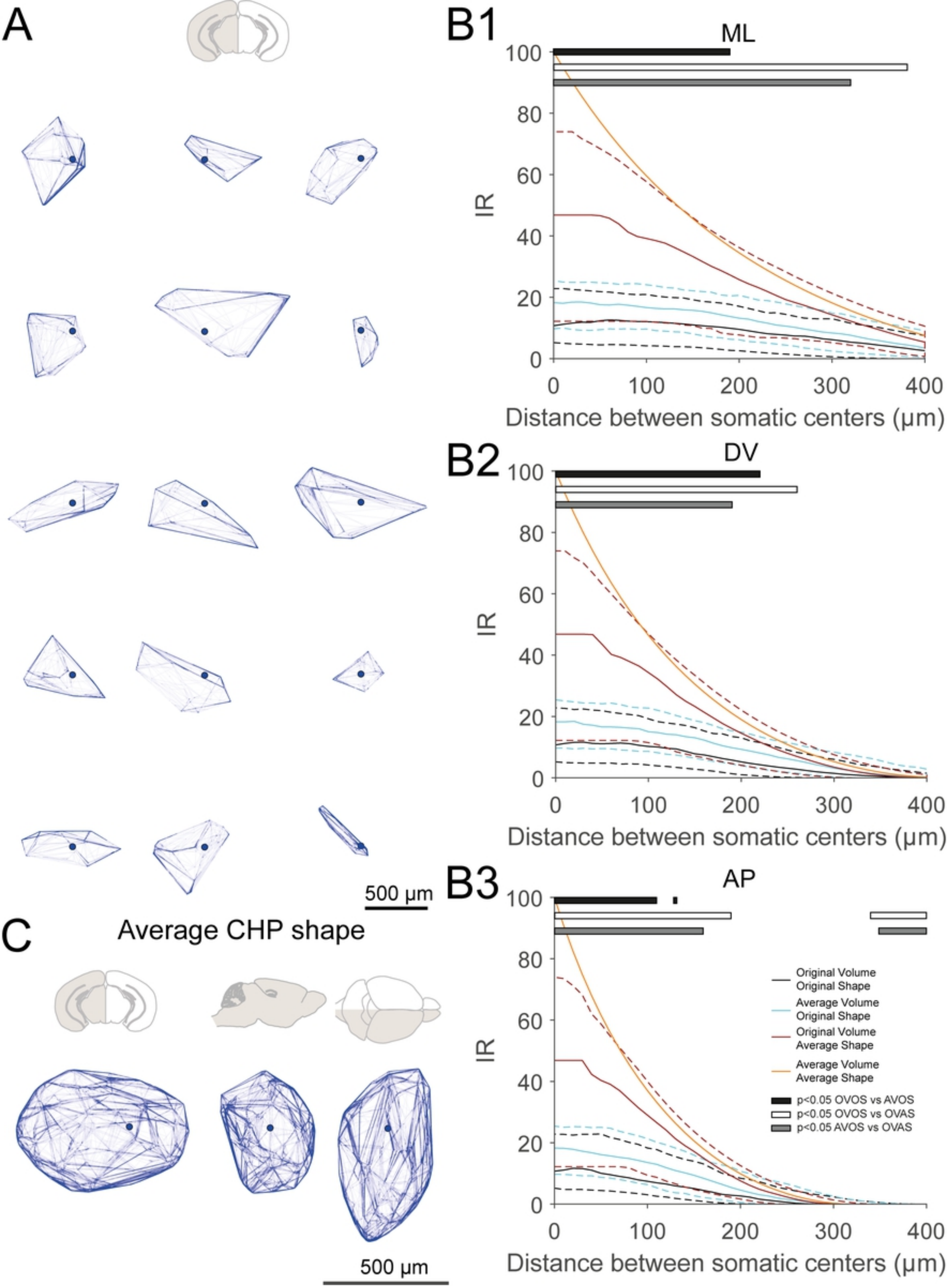
A
B1
ML
IR
Distance between somatic centers (µm)
B2
DV
IR
Distance between somatic centers (µm)
B3
AP
IR
Distance between somatic centers (µm)
Original Volume
Original Shape
Average Volume
Original Shape
Original Volume
Average Shape
Average Volume
Average Shape
p<0.05 OVOS vs AVOS
p<0.05 OVOS vs OVAS
p<0.05 AVOS vs OVAS
500 µm
C
Average CHP shape
500 µm

Fig 10

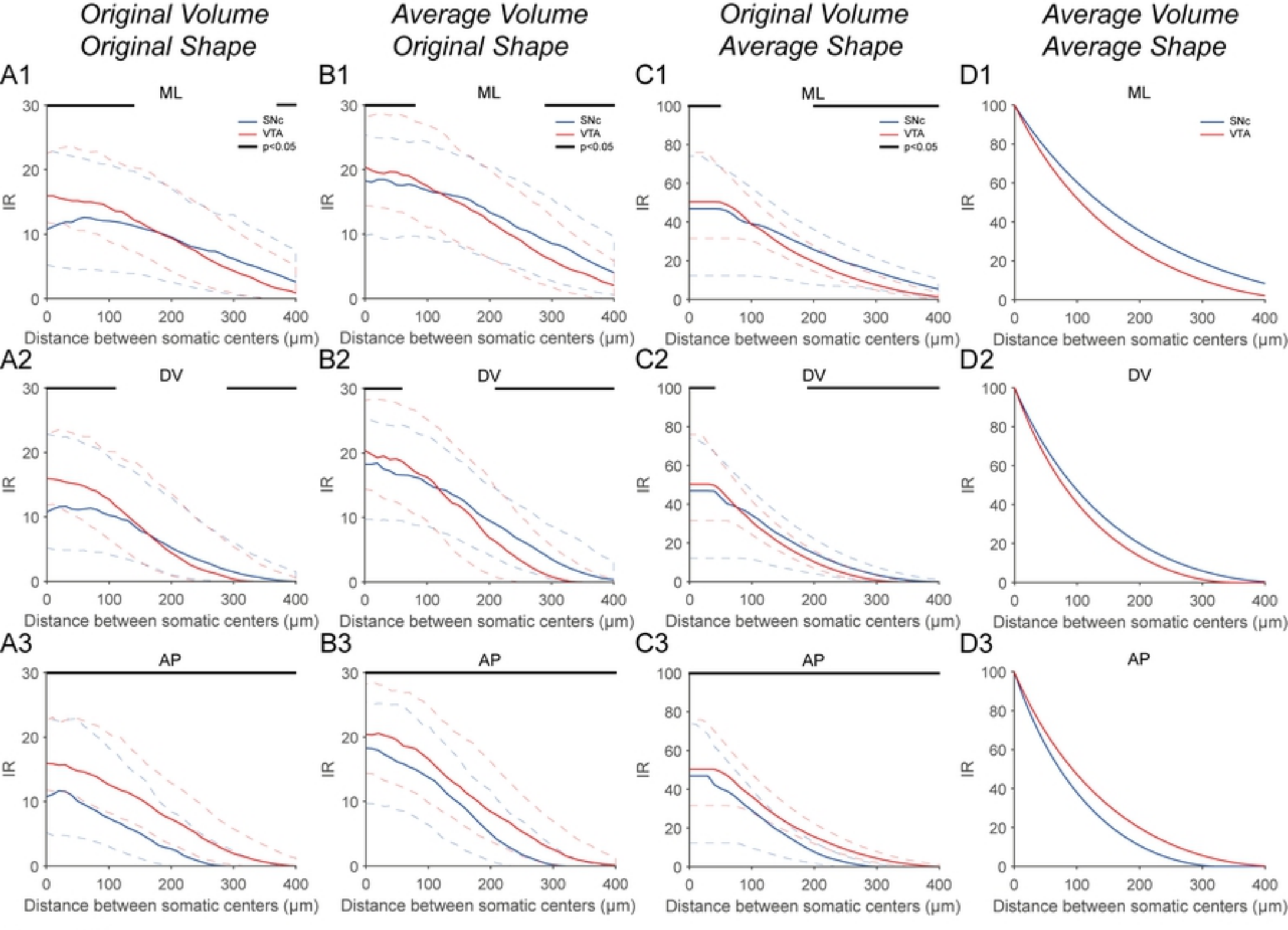
Original Volume
Original Shape
Average Volume
Original Shape
Original Volume
Average Shape
Average Volume
Average Shape
A1
B1
C1
D1
A2
B2
C2
D2
A3
B3
C3
D3
ML
DV
AP
SNc
VTA
p<0.05
IR
Distance between somatic centers (μm)

Fig 11